nature portfolio

https://doi.org/10.1038/s41586-022-04713-1

Supplementary information

Single-cell eQTL models reveal dynamic T cell state dependence of disease loci

In the format provided by the authors and unedited

Single-cell eQTL models reveal dynamic T cell state-dependence of disease loci

Aparna Nathan[1–5], Samira Asgari[1–5], Kazuyoshi Ishigaki[1–5], Cristian Valencia[1–5], Tiffany Amariuta[6], Yang Luo[1–5], Jessica I. Beynor[1–5], Yuriy Baglaenko[1–5], Sara Suliman[2], Alkes Price[4,6,7], Leonid Lecca[8,9], Megan B. Murray[8,10], D. Branch Moody[2], Soumya Raychaudhuri[1–5,11,*]

Table of Contents

Supplementary Note

Single-cell CITE-seq data generation (Nathan, et al. 2021 *Nature Immunology*)

The single-cell CITE-seq data used in this study were previously published in Nathan, et al[25]. Summaries of data collection and processing steps are in **Methods**.

In greater detail, upon sample collection, we purified PBMCs with Ficoll-Hypaque and cryopreserved them (5 million cells/mL). For the CITE-seq experiment, we processed 276 samples from 264 donors. For each sample, we thawed 10 million cells, added dropwise to prewarmed complete RPMI (cRPMI; RPMI 1640 supplemented with 10% heat-inactivated fetal bovine serum (FBS; Gemini), nonessential amino acids (Gibco), 2-mercaptoethanol (Gibco), penicillin–streptomycin (Gibco) and l-glutamine (Gibco)), washed, and resuspended in 1 mL cRPMI.

Then, we negatively isolated memory T cells with a Pan T cell magnetic-activated cell sorting (MACS^{R}) kit with anti-CD45RA biotin added (using 2x reagents, ~98.4% purity). We followed an optimized version of the CITE-seq protocol with TotalSeq^{TM}-A (BioLegend) oligonucleotide-labeled antibodies to stain up to 300,000 cells per sample[57]. We used FcX True Stain (BioLegend) with 0.2 μg μl−1 dextran sulfate sodium (Sigma-Aldrich, RES2029D-A707X) in labeling buffer (PBS pH 7.4 with 1% UltraPure BSA for 10 min at 4 °C. Then, we added an oligonucleotide-labeled antibody mix containing TotalSeq-A (BioLegend) anti-CCR6 in 10 μl of labeling buffer and incubated at room temperature for 25 minutes, followed by staining with 30 other TotalSeq-A antibodies for 25 minutes at 4 °C. We washed cells sequentially with 2 ml, 1 ml and 1 ml of labeling buffer and passed each sample through a 40-μm filter.

We sorted up to 10,000 live cells per sample on a BD FACSAria Fusion cell sorter, removing non-lymphocytes and dead cells with forward and side scatter gating. After 10x Genomics library preparation on batches of six samples, we sequenced pairs of libraries on an Illumina HiSeq X with 400 million reads per lane and paired-end 150 base-pair reads.

Single-cell CITE-seq data quality control (Nathan, et al. 2021 *Nat Imm*)

We used Cell Ranger mkfastq and count to align reads to GRCh38 and detect cells (n=725,199). We then used Demuxlet to demultiplex samples in each batch of six based on 738,194 genotyped and imputed SNPs (INFO = 1) and identify singlets (n=640,966, ~12% doublets)[58]. Next, we removed cells with fewer than 500 genes expressed or more than 20% of UMIs from mitochondrial genes (n=518,032 cells remaining). We removed five donors whose genotypes called from single-cell RNA-seq did not match array-based genotypes (n=514,835 cells remaining). Finally, we removed outlier non-memory T cells based on CITE-seq surface protein expression (n=500,089 CD3+CD45RO+ cells remaining for further analysis.) After normalization, scaling, and PCA (**Methods**), we used Harmony to correct for donor and library preparation batch effects[59].

Genetic data quality control (Luo, et al. 2019 *Nat Comm*)

In Luo, et al., we genotyped 4,002 people from a Peruvian tuberculosis progression cohort[26]. We used a custom Affymetrix array (LIMAArray) designed for this Peruvian cohort based on whole exome sequencing of 116 Peruvian individuals. We

called genotypes across all samples using apt-genotype-axiom and excluded duplicates (identity-by-state > 0.9), TB index cases diagnosed at age > 40, and outliers based on excess of heterozygosity (≥3.5 standard deviations) or genetic ancestry. The 259 samples in this study are a subset of the samples passing quality control in Luo, et al.

Global genetic ancestry analysis (Asgari, et al. 2020 *Nature*; Nathan, et al. 2021 *Nat Imm*)

As previously described, to estimate the proportions of global ancestry components, we first combined genotyping data for these samples with data from 1000 Genomes Project Phase 3 (2,054 individuals from 26 populations), Siberians (245 individuals from 17 populations), and Native Americans (493 individuals from 57 populations) by matching variants with MAF > 1% on position, reference, and alternate allele[30]. Using PLINK, we performed PCA and removed highly correlated variants (r^2 > 0.1, --indep-pairwise 50 10 0.1)[60]. Then, we used ADMIXTURE (K = 4) to infer global genetic ancestry proportions[61].

Comparison to published bulk T cell eQTLs

We compared lead variants' effects to published bulk memory CD4+ T cell eQTLs from individuals mostly of European or Asian self-reported ancestry in the Database of Immune Cell eQTLs (DICE, n=91) to assess directional concordance for eQTLs that both studies were powered to detect[31]. We meta-analyzed eQTL effects across six flow-sorted memory CD4+ T cell subsets (T_{reg}, T_H1, $T_H1/17$, T_H17, T_H2, T_{FH}). Despite ancestry and technology differences, most of the eQTLs identified in single-cell

memory T cells were also nominally significant in this bulk study without multiple testing correction (2,214 significant at meta-analysis p<0.05 in DICE/3,162 significant in single-cell study and measured in DICE); those that were significant in both datasets had mostly concordant directions of effect (2,094/2,214=93%, **Extended Data Fig. 2a**). A minority of eQTLs were found exclusively in the single-cell study, as expected given that other studies have demonstrated reduced power of pseudobulk eQTL discovery compared to bulk[53]. Fewer eQTL effects were shared with naïve CD4+ T cells in DICE, but effects were still largely concordant (1,227/1,293=95%). Therefore, we also compared lead variants' effects to published bulk naïve CD4+ T cell eQTLs from a larger study of individuals of European ancestry (BLUEPRINT, n=169)[27]. Again, we observed similarly high concordance (at q<0.05, 2,056 significant in both/3,249 significant in single-cell study and measured in BLUEPRINT; 1,917/2,056=93% same direction of effect, **Extended Data Fig. 2b**).

Power to replicate pseudobulk eQTLs in single-cell model

Previous studies have reported limited power to replicate bulk eQTLs with single-cell resolution models. We downsampled cells from the memory T cell dataset and identified eQTLs using the single-cell PME model. We observed through downsampling that replication of bulk eQTLs improves with increasing cell count (**Supplementary Fig. 4d**)[53].

Comparing LME and PME

Effects were concordant between LME and PME models but significance varied, especially for more sparsely expressed genes (**Supplementary Fig. 7a-c**). LME reported lower standard errors when estimating interaction effects for more sparse genes, while PME reported less confidence in its estimates (**Supplementary Fig. 7d,e**). CD4-dependent eGenes from LME are significantly more differentially expressed and sparse than those from PME **(Extended Data Fig. 3d-f).**

Genetic ancestry and cell state

In previously published analyses in this dataset, genetic ancestry was significantly associated with cell state composition, namely Native American genetic ancestry and expanded cytotoxic CD4+ cells[25]. Here, we observe nominal association between genotype PCs 1 and 2 (correlated with Native American or European ancestry, **Supplementary Fig. 2a,b**) and CVs 3 and 5 that distinguish cytotoxic CD4+ T cells (all multivariate regression betas' Wald p > Bonferroni threshold .05/100, **Supplementary Fig. 2d,e, Supplementary Fig. 3a,b**). No CVs were significantly associated with genotype PCs, and by including genotype PCs in the model we could more robustly test whether state-dependent eQTLs explained variance in gene expression beyond cell-state shifts due to genetic background.

Simulated null for PME interaction model

For a representative subset of 12 eGenes—including those with and without significant interactions—we assessed calibration more rigorously by calculating interaction p values against a simulated null model (**Methods)**[62]**.** We observed high

concordance between empirical p values and the LRT p values (**Supplementary Fig. 8e**).

Comparing Poisson and negative binomial interaction models

Negative binomial models are also a common strategy to model UMI counts in case of overdispersion, but require an additional parameter and are more computationally expensive[53,63]. In this dataset, we find—as previous studies have shown—that genes are mostly not overdispersed (**Supplementary Fig. 9a**)[33]. Thus, when we randomly sampled 500 eGenes with and 500 eGenes without significant CV1 interactions, we observed high concordance between their z scores and significance measures between Poisson and negative binomial models, justifying the use of the simpler and faster Poisson model (**Supplementary Fig. 9b,c, Supplementary Table 17**).

Cell-state dependence of non-pseudobulk-significant eQTLs

We also tested eGenes and their lead variants that were not significant in pseudobulk analysis and found a smaller proportion with state-dependent effects (390/8,692 at q<0.05, **Supplementary Table 34**). For example, a *TIGIT* eQTL was not significant in pseudobulk (p = 0.17) but had strong effects in regulatory or central-memory-like CD4+ cells phenotypes, compared to CD8+ cells with higher average *TIGIT* expression (LRT interaction p = 4.76×10^{-28}, **Supplementary Fig. 11**). To minimize multiple testing burden and focus on more robust candidates, we limited further analyses to pseudobulk-significant eGenes and their lead variants.

GO term enrichment of lead and secondary variants

eGenes interacting with CVs were often enriched for relevant functions—for example, eGenes interacting with CV1 in the multivariate model were strongly enriched for the Gene Ontology terms corresponding to *immune effector process* (GO:0002252, OR=2.5, Fisher $p=5.33 \times 10^{-15}$) and *innate immune response* (GO:0045087, OR=2.6, $p=3.28 \times 10^{-11}$), in concordance with CV1's hypothesized innate/effector-like state (**Supplementary Table 40**). But in some cases, lead and secondary eQTLs had discordant functional enrichments: only CV6-dependent secondary eQTLs were enriched for *leukocyte-mediated cytotoxicity* (GO:0001909, OR=40.3, $p=4.04 \times 10^{-3}$), unlike the lead eQTLs (OR=2.4, p=0.15). This suggests that secondary eQTL signals may still shape key cellular functions with potential disease relevance.

Modeling continuous cell states with mRNA or protein PCs

When we conducted a multivariate eQTL interaction analysis using single-modality PCs to define continuous cell states, we identified comparable numbers of eGenes that interact with the first seven mRNA or protein PCs (mRNA:2,364, protein:1,915, $q<0.05$, **Supplementary Fig. 12a, Supplementary Tables 37** and **38**). The majority of state-dependent eGenes from the multimodal CV analysis were also significantly associated with mRNA or protein PCs (1,446/2,117=68%, **Supplementary Fig. 12b**), and we observed some concordance between interactions with individual CVs and PCs (**Supplementary Fig. 12c,d**). In this dataset, we have previously shown that CVs define biologically relevant cell states not discriminated by mRNA PCs[25].

Furthermore, CVs' unique interpretability and robustness bolsters state-dependent eQTL analyses because they incorporate a panel of memory T cell state-defining surface proteins; thus they are less susceptible to technical confounders and more likely to point to interpretable biology.

Modeling state-dependent eQTLs in a heterogeneous context

Here, we have demonstrated that a single-cell PME model identifies eQTLs that vary with continuous T cell states. We also applied the model to other cell types. First, we used a published PBMC dataset, which offers mixed cell types in contrast to a single cell type[24]. There were 108,209 unstimulated PBMCs from 89 whole-genome-sequenced male donors, and >99% of cells per donor, on average, had been classified in the original study as monocytes, CD4+ and CD8+ T, B, or NK cells (**Supplementary Fig. 13a**). We confirmed these annotations with canonical markers (**Supplementary Fig. 13b**).

To identify state-dependent eQTLs, we first defined 962 pseudobulk PBMC eQTLs ($q<0.05$, **Methods**) to test for state-dependent effects in the single-cell PME model. We modeled cell states in two distinct ways: (1) one multivariate model with six expression PCs defined across all the PBMCs as the cell state interaction terms, or (2) separate univariate models for each of the five cell states, each with one binary cell state term. Continuous PCs were highly correlated with individual cell types: for example, PC1 separated monocytes from other cell types (**Supplementary Fig. 13c**). As a result, although each of the cell types and PCs was associated with a set of state-dependent eQTLs (**Supplementary Fig. 13d,e**), the set of 369 significant state-

dependent eQTLs identified in the multivariate PC model largely overlapped with the pooled set of 370 state-dependent eQTLs from the five univariate cell type models (292 shared state-dependent eQTLs; **Supplementary Fig. 12f, Supplementary Tables 43** and **44**).

Moreover, eQTL interactions were especially shared between PCs and the cell types that they correlated with. For example, nearly all the PC1-dependent and monocyte-dependent eQTLs were shared, including an eQTL for *EIF5A* that was weaker in monocytes or cells with low PC1 score (**Supplementary Fig. 13g,h**). Although PC3 did not recapitulate all the eQTLs associated with B cells—its most correlated cell type—an eQTL for *SERPINB6* that was nearly absent in B cells was also weakest in the lowest third of PC3 scores (**Supplementary Fig. 13i,j**). These results demonstrate that the dominant regulatory variation in heterogeneous tissues, which is between discrete cell types, can still be modeled at single-cell resolution.

Modeling state-dependent eQTLs in a granular context

We selected CD4+ T cells and CD8+ T cells based on surface protein expression and used CCA to define canonical variates within each compartment. The cell states represented by these two sets of CVs appear distinct: for example, T_H2 cells are a subset of CD4+ cells driven by GATA3 transcription factor and expressing CRTH2, and we only observed a CV correlated with these markers in the CD4 analysis (CD4-CV3, **Supplementary Fig. 14a,c**). Among CD8+ T cells, we instead see axes correlated with markers of variable CD8+ cytotoxicity such as *GNLY*, *CD27*, and granzymes. CD8-CV6 correlated with markers of mucosal-associated invariant T cells, a distinct CD8+

population (**Supplementary Fig. 14b,d**)[64]. The sub-CD4 and sub-CD8 CVs correlated with the CVs defined across all memory T cells—especially with CV1 and CV2 (**Supplementary Fig. 14e,f**). However, correlations were lower in the CD8+ compartment because these cells were less abundant in the dataset (~430K CD4+, ~56K CD8+) and may have contributed less to overall variation.

Then, we tested the 6,511 pseudobulk-significant eQTLs defined across all memory T cells for interactions with the top six CVs from each compartment. Adjusting for the same covariates as in the memory analysis, we found 1,728 and 350 eQTLs varied with sub-CD4 and sub-CD8 states (**Supplementary Tables 45** and **46**). Ninety percent of the interactions identified in each sub-state analysis were also identified in the memory analysis, but 180 eQTLs only had sub-state-dependent effects. Although power to detect interactions with sub-CD8 states was limited by low cell count, examples like the two state-dependent eQTLs only associated with CD8-specific CV4 and not associated with any mRNA or memory CVs suggest that with larger cell counts, continuous states defined within subtypes may reveal cell-type-specific regulatory heterogeneity.

eQTL interactions with an interferon-correlated trajectory

From each of the 89 donors in the PBMC dataset, we selected monocytes from both mock-treated and IAV-exposed samples (n=24,783 cells total) and corrected effects of sample, batch, and infection condition (**Supplementary Fig. 15a**). We constructed a trajectory with DDRTree and computed pseudotime along this trajectory with a principal curve (**Supplementary Fig. 15b**)[65,66]. The proportion of IAV-exposed

cells increased (**Supplementary Fig. 15c**), and the expression of interferon- and viral-response genes such as *CXCL10* and *APOBEC3A* also increased along the trajectory (Pearson r=0.59 and 0.55, respectively; **Supplementary Fig. 15d,e**), suggesting that the trajectory captured an interferon-response gradient[67-69].

We pooled eQTLs identified in pseudobulk analysis of unstimulated monocytes or unstimulated PBMCs to define a set of 997 eQTLs to test for interactions with the trajectory in the single-cell PME model, adjusting for donor covariates, technical confounders, and random effects for donor and batch (**Methods**). Despite analyzing a relatively small number of cells, we identified 48 eQTLs with effects that varied significantly along the trajectory (q<0.05, **Supplementary Table 47**). Only five remained upon permutation of trajectory, demonstrating low type I error. The rs2269524 eQTL for *SMDT1* was one trajectory-dependent example that decreased in magnitude along the trajectory (β_{GxTraj}=0.054, p=3.42x10^{-5}; **Supplementary Fig. 15f**); in a previous bulk study of whole blood, we observed an interferon-dependent decrease in effect for a closely linked eQTL variant in the same locus (rs2859438, r^2 = 0.97 in 1KG PEL)[7].

eQTL interactions with disease cell states through reference mapping

We used Symphony to project the memory T cell dataset of 500,089 blood memory T cells from 259 donors onto a reference of almost 70,000 colon T cells from Smillie et al., who assayed 30 ulcerative colitis (UC) patients and healthy donors (**Supplementary Fig. 16a**)[70,71]. Despite study differences, we observed T cells with similar phenotypes mapping close together, such as CD8+ T cells from both datasets (**Supplementary Fig. 16b,c**).

In the original study, Smillie, et al. identified a potentially pathogenic CD8+ T cell expressing IL-17 that was expanded in people with UC. Upon closer inspection of the colon cells, we observed that PC4 separated the IL-17+ population from the other CD8+ cells (**Supplementary Fig. 16d**), suggesting this axis's disease relevance. We used the single-cell PME model to test interactions between the 6,511 eQTLs from the memory T cell analysis and the cell states defined by the UC-PCs. We modeled the expression of each eGene across the 500,089 memory T cells as a function of the cells' own genotypes and covariates, their scores on a UC-PC, and the interaction between that score and genotype. Despite modest correlations between UC-PCs and memory T cell CVs, when we tested each of the top four UC-PCs, we observed substantial state-dependence and recapitulated many interacting eQTLs from the memory T cell analysis (**Supplementary Fig. 16e,f, Supplementary Table 48**). There were, however, some eQTLs that only had interactions with UC-PCs. These may reflect tissue- or disease-specific state dependence. For UC-PC4, 124/541 state-dependent eQTLs were UC-specific, including eQTLs for *PARP14* and *FBXO7* (**Supplementary Fig. 16g,h**). This suggests their effects might vary between healthy T cell states and the CD8+ IL-17+ state, with implications in disease.

Methods

Single-cell RNA-seq and genotype data and quality control (QC)

We previously published a dataset of memory T cells from a 259-donor subset of a Peruvian tuberculosis disease progression cohort (128 former cases, 131 former latently infected controls; GEO: GSE158769) along with detailed sample processing methods[25,72]. Briefly, we negatively isolated memory T cells with a modified Pan T cell magnetic-activated cell sorting (MACS^R) kit with anti-CD45RA biotin and followed an optimized version of the CITE-seq protocol with TotalSeq^{TM}-A (BioLegend) oligonucleotide-labeled antibodies for a panel of 31 surface proteins[57]. We pooled cells into batches of six donors for 10x Genomics library preparation and sequenced on an Illumina HiSeq X. Reads were aligned to GRCh38 with Cell Ranger. After demultiplexing donors with Demuxlet, we removed cells labeled as doublets, with < 500 genes expressed or > 20% of unique molecular identifiers (UMIs) from mitochondrial genes, from samples whose genotypes did not match genotypes called from single-cell data, or lacking surface markers of memory T cells (CD3 and CD45RO)[57].

A superset of 4,002 donors was genotyped in a separate genetic study on a custom Affymetrix array (LIMAArray) based on whole exome sequencing from 116 individuals with active TB from the same Peruvian cohort (**Supplementary Note;** dbGaP: phs002025). The design of this array has been described previously[26]. We excluded donor outliers based on genotyping quality and genetic ancestry. After calling genotypes for all 4,002 donors with the apt-genotype-axiom program, we removed variants that were significantly associated with batch ($p < 1 \times 10^{-5}$), duplicated, or had low call rate (< 95%), significant differences in the missingness rate between cases and

controls (> 10^{-5}), or Hardy-Weinberg p value < 10^{-5} in controls. After QC, 675,358 genotyped variants remained.

We mapped variants to GRCh37/b37 and used SHAPEIT2 to pre-phase genotypes and IMPUTE2 to impute genotypes with 1000 Genomes Project Phase 3 as the reference panel[73,74]. To calculate genotype principal components, we combined autosomal genotyping data from the full cohort (n = 4,002) with whole-genome sequencing data from the 1000 Genomes Project Phase 3 (n=2,045 people from 26 populations), and with PLINK, matched variants with MAF > 1% on position, reference, and alternate allele and removed highly correlated variants (r^2 > 0.2, --indep-pairwise 50 5 0.2)[60]. Then, we conducted PCA with PLINK (--pca).

After removing SNPs with an INFO score < .9, minor allele frequency < 0.05, or deletions, the remaining variants were converted to GRCh38 with liftOver. After single-cell and genotype QC, we used 500,089 cells from 259 donors and 5,486,956 variants for eQTL analysis.

Single-cell data processing

mRNA and protein data were processed separately, as described[25]. Briefly, we normalized the UMIs for each gene in each cell to log(counts per 10,000) and used centered-log-ratio normalization for each protein within each cell. Normalized mRNA and protein expression were scaled so that each feature had mean = 0, variance = 1 across all cells. After selecting the top 1,000 variable genes per donor and removing the mouse immunoglobulin G protein (control), we conducted principal component analysis of each modality with the irlba R package and corrected the top 20 PCs of each modality for donor and library preparation batch effects with Harmony[59].

Pseudobulk eQTL analysis

To make pseudobulk expression profiles for 259 donors, we removed cells from 12 technical replicate samples and summed the UMI counts for each gene across all cells from each donor, producing one aggregated expression value for each gene in each donor. For CD4+ and CD8+ pseudobulk analysis, we constructed pseudobulk expression profiles for each donor in each compartment by *in-silico* gating cells that were CD4+CD8- or CD8+CD4-, respectively, based on their normalized surface protein expression measured in CITE-seq. Gates were defined through visual inspection. For T_{reg} pseudobulk analysis, we used previously defined cluster annotations to construct a pseudobulk expression profile for the cells in clusters C-5 (*RORC*+ T_{reg}) and C-9 (T_{reg})[25].

Genes were removed if expressed in fewer than half the donors (pseudobulk counts > 0 in ≤ 129 donors). For the remaining 15,789 genes, we normalized the pseudobulk profiles to $\log_2$(counts per million + 1) and applied inverse normal transformation. Then, we used probabilistic estimation of expression residuals (PEER) implemented in R to regress out age, sex, five genotype PCs (68% of the genetic variance explained by the top 20 genotype PCs**, Supplementary Fig. 2c**), and up to 45 PEER factors based on previously published optimization by GTEx[29,75]. The number of effective factors is reduced by PEER's regularization strategy, which selects weights such that the overall contribution of less-relevant factors is close to 0 (**Supplementary Fig. 1d**). Age was calculated for the time of blood draw.

We then conducted a whole-genome eQTL analysis for all 22 autosomal chromosomes. For each gene, we associated its residual expression after PEER normalization with the dosage at each SNP within 1 MB of the transcription start site.

These models were implemented in FastQTL (default settings)[76]. To ensure robustness, we used FastQTL's beta approximation to compute a permutation p value from 1,000 permutations. To correct for multiple hypothesis testing, we calculated Storey q values for the lead SNP for each gene, and identified eGenes with significant eQTL variants with $q < 0.05$ (with qvalue R package)[77].

For conditional pseudobulk analysis, we iteratively regressed each eGene's PEER-normalized residuals on the dosage of its lead SNP and used the subsequent values for FastQTL analysis. We repeated this twice.

Comparison to DICE

We used the eQTL summary statistics reported by DICE from bulk analysis of six sorted memory T cell subsets: memory T_{reg}, T_H1, $T_H1/17$, T_H17, T_H2, T_{FH} (downloaded from https://dice-database.org/downloads)[31]. We selected eGenes that were significant in our dataset (n = 6,511) and used inverse-variance-weighted meta-analysis to compute aggregate betas, standard deviations, and z scores across the K = 6 cell states in DICE:

$$\beta_{meta} = \frac{\sum_{k=1}^{K} \frac{\beta_k}{se_k^2}}{\sum_{k=1}^{K} \frac{1}{se_k^2}}$$

$$se_{meta} = \frac{1}{\sum_{k=1}^{K} \frac{1}{se_k^2}}$$

$$z_{meta} = \frac{\beta_{meta}}{se_{meta}}$$

We compared the direction of these meta-analysis z scores with the pseudobulk z scores from the single-cell memory T cell dataset.

For heterogeneity analysis, we calculated two statistics: (1) a Cochran's Q statistic across K= 6 subsets assayed in DICE ($Q = \sum_{k=1}^{K} \frac{1}{se_k^2}(\beta_k - \beta_{meta})^2$) and I^2 ($\frac{Q-df}{Q}$x100%).

Comparison to BLUEPRINT

We used the eQTL summary statistics reported by BLUEPRINT from bulk analysis of sorted naïve CD4+ T cells, monocytes, and neutrophils[27]. We selected eGenes that were significant in our dataset (n = 6,511) and, for each BLUEPRINT cell type, identified the subset of eGene/lead variant pairs also measured by BLUEPRINT and significant in both datasets at q < 0.05 (n = 2,056 for naive CD4+ T cells, 1,651 for monocytes, and 1,312 for neutrophils). We compared the direction of effect for these variants between the two datasets.

Continuous cell state definition and annotation

For multimodal dimensionality reduction, we used canonical correlation analysis, as implemented in the cc function from the CCA R package[78]. We ran CCA on scaled mRNA expression for the most variable genes (excluding T cell receptor genes) and scaled protein expression for all 30 memory T cell proteins, and computed cells' scores on each canonical variate (CV) based on the weight of each gene on each CV. We then corrected scores on the top 20 CVs for donor and batch effects. For visualization, we projected this embedding into a two-dimensional Uniform Manifold Approximation Projection (UMAP) with the umap function from the uwot R package[79].

To annotate each CV based on its biological correlates, we first measured the Pearson correlation coefficient between cells' CV scores and the normalized expression

of each surface protein marker in the protein panel. We measured correlations between CV scores and the normalized expression of genes encoding lineage-defining genes.

We also conducted gene set enrichment analysis. First, we measured the correlation of each CV prior to batch correction with the expression of each gene used as input for CCA. These correlations defined the ranked gene list for each CV. Then, we measured the enrichment of each immunologic gene set (C7, only those annotated as "UP") in MSigDB and a published "innateness" gene list in each CV's ranked gene list with the fgsea function in the fgsea R package[80-82]. We corrected for multiple hypothesis testing with a Bonferroni p value threshold adjusted for 2,360 gene sets tested ($0.5/2{,}360 = 2.12 \times 10^{-5}$).

To compare CV scores between and within clusters, we used the cluster annotations defined in the previous study and computed the average score on each CV for cells from each cluster. We also randomly selected two cells each from clusters C-3 and C-15 to compare to each other and the cluster.

We repeated CCA within only CD4+ and CD8+ T cells. We isolated each lineage based on surface protein gates as described above for pseudobulk analysis and identified the most variable genes within each batch based on dispersion (2974 genes total for CD4+, 5225 for CD8+). We scaled these genes and cosine-normalized them. We also selected the most informative proteins for each lineage based on high Kullback-Leibler divergence: comparing the distribution of cells with high protein expression (>85th percentile) to the distribution of all cells (KL > KL for lineage marker). We removed TCR genes due to lower quality mapping and ran CCA to compute cells' scores on each CV within each lineage. We corrected the top 20 CVs for donor and

batch effects with Harmony and projected cells into a two-dimensional embedding with UMAP. As with the memory T cell CVs, we measured the correlation between CVs and the normalized expression of key lineage-defining genes.

Single-cell eQTL modeling

We modeled single-cell eQTLs with a Poisson model of each gene's UMI counts as a function of genotype at the eQTL variant and other donor- and cell-level covariates, for each gene:

$$\log(E_i) = \theta + \beta_G X_{d,geno} + \beta_{age} X_{d,age} + \beta_{sex} X_{d,sex} + \beta_{nUMI} \log(X_{i,nUMI}) + \beta_{MT} X_{i,MT} + \sum_{k=1}^{5} \beta_{gPC_k} X_{d,gPC_k} + \sum_{k=1}^{5} \beta_{ePC_k} X_{i,ePC_k} + (\phi_d \mid d) + (\kappa_b \mid b)$$

where *E* is the expression of the gene in cell *i*, θ is an intercept, and all other βs represent fixed effects as indicated (nUMI = number of UMI, MT = proportion of mitochondrial UMIs, gPC= genotype PC, ePC=single-cell mRNA expression PC pre-batch correction) for covariates in cell *i*, donor *d*, or batch *b*. Donor and batch are modeled as random effect intercepts.

To test interactions with cell state, we added a fixed effect for cell state and a cell state x genotype interaction term (referred to as the univariate model):

$$\log(E_i) = \theta + \beta_G X_{d,geno} + \beta_{age} X_{d,age} + \beta_{sex} X_{d,sex} + \beta_{nUMI} \log(X_{i,nUMI}) + \beta_{MT} X_{i,MT} + \sum_{k=1}^{5} \beta_{gPC_k} X_{d,gPC_k} + \sum_{k=1}^{5} \beta_{ePC_k} X_{i,ePC_k} + \beta_{cell\ state} X_{i,cell\ state} + \beta_{Gxcell\ state} X_{d,geno} X_{i,cell\ state} + (\phi_d \mid d) + (\kappa_b \mid b)$$

When testing whether the discrete state (CD4+) or the continuous state (CV1) captured more variance, we included cell state and cell state interaction terms for both and

removed each interaction term to create the corresponding null model for the likelihood ratio test (described below).

To test interactions with former TB progression status, we used the same model but with a fixed effect and genotype-interaction term for TB status.

To test interactions with multiple state-defining covariates (e.g., multiple CVs), we included additive fixed effect and interaction terms for each CV (referred to as the multivariate model):

$$\log(E_i) = \theta + \beta_G X_{d,geno} + \beta_{age} X_{d,age} + \beta_{sex} X_{d,sex} + \beta_{nUMI} \log(X_{i,nUMI}) + \beta_{MT} X_{i,MT} + \sum_{k=1}^{5} \beta_{gPC_k} X_{d,gPC_k} + \sum_{k=1}^{5} \beta_{ePC_k} X_{i,ePC_k} + \sum_{k=1}^{n} \beta_{CV_k} X_{i,CV_k} + \sum_{k=1}^{n} \beta_{GxCV_k} X_{d,geno} X_{i,CV_k} + (\phi_d \mid d) + (\kappa_b \mid b)$$

To test eQTLs within discrete cell states (e.g., CD4+), we subsetted the full dataset to cells in the state of interest (using gates or clusters). Then, we ran the Poisson single-cell model without any cell state terms.

We fit all single-cell Poisson mixed models with the glmer function in the lme4 R package, with family="poisson", nAGQ=1, and control=glmerControl(optimizer = "nloptwrap")[83]. To determine the significance of this model, we used a likelihood ratio test comparing the models with and without the genotype term (for the memory T cell analysis) or the cell state interaction term(s) (for the cell-state-specific analyses) and calculated a p value for the test statistic against the Chi-squared distribution with one degree of freedom. We corrected for multiple hypothesis testing by calculating Storey q values across all tested eQTLs[77]. To compare significance between models, we used a statistic based on the LRT p value, I^{-1}(LRT p/2)*sign(beta): determine the upper critical value for the LRT p value, then adjust the sign to match beta's sign. To compare effect

sizes for terms between models, we used Wald statistic z scores (beta/standard error) for the term of interest.

For comparison, we also used a single-cell linear mixed effects (LME) model to test eQTLs across all memory T cells and for state dependence with CD4+ state or continuous CV1. The model included the same covariates as the Poisson models. For example, across all memory T cells:

$$G_i = \theta + \beta_G X_{d,geno} + \beta_{age} X_{d,age} + \beta_{sex} X_{d,sex} + \beta_{nUMI} \log(X_{i,nUMI}) + \beta_{MT} X_{i,MT} + \sum_{k=1}^{5} \beta_{gPC_k} X_{d,gPC_k} + \sum_{k=1}^{5} \beta_{ePC_k} X_{i,ePC_k} + (\phi_d \mid d) + (\kappa_b \mid b)$$

where *G* is the log2(counts per 10K) normalized expression of the gene in cell *i*. We fit all single-cell linear mixed models with the lmer function in the lme4 R package, with REML = F and determined the significance of the model as described for Poisson models.

We also tested multivariate PME interaction models with 7 mRNA PCs, 7 protein PCs, 6 CD4-CVs, or 6 CD8-CVs (all defined above, post-batch correction). The models contained the same covariates as the all-memory-T cell model, and we used an LRT and q values ($q < 0.05$) to determine significance.

We also used a single-cell negative binomial mixed effects model to test eQTL interactions with CV1 for a subset of 500 genes with significant CV1 dependence and 500 randomly sampled genes without significant CV1 dependence in the PME model. The model included the same covariates as the Poisson models. We fit all negative binomial mixed models with the glmer.nb function in the lme4 R package, with nAGQ=1 and control=glmerControl(optimizer = "nloptwrap") and determined the significance of the model as described for Poisson models.

Type I error estimation

To estimate the false positive rate for the single-cell PME model of memory T cell eQTLs, we permuted genotype across donors and ran the PME model once for each gene (n = 6,511). Then, we used a likelihood ratio test to compute a p value for each gene under the permutation, pooled these permutations across genes, and measured the proportion of trials with a p value < alpha = 0.05. To estimate the false positive rate for the single-cell PME model of cell state-dependent eQTLs, we used the same permutation approach but permuted cell state across cells to preserve the main genotype effect.

For further evidence of model calibration, we simulated data under the null hypothesis, as previously described by Buzkova, et al., to calculate empirical p values for the CV1 interaction[61]. Briefly, for each gene, we fit the null model:

$$\log(E_i) = \theta + \beta_G X_{d,geno} + \beta_{age} X_{d,age} + \beta_{sex} X_{d,sex} + \beta_{nUMI} \log(X_{i,nUMI}) + \beta_{MT} X_{i,MT} + \sum_{k=1}^{5} \beta_{gPC_k} X_{d,gPC_k} + \sum_{k=1}^{5} \beta_{ePC_k} X_{i,ePC_k} + \beta_{CV1} X_{i,CV1} + (\phi_d \mid d) + (\kappa_b \mid b)$$

We used the beta estimates from this model to predict the expression of the gene in each cell under the null hypothesis (i.e., no cell-state interaction effect). With these estimates as the lambda, we sampled 1,000 expression values for each cell to construct 1,000 null datasets of 500,089 cells. For each null dataset, we fit the full model:

$$\log(E_i) = \theta + \beta_G X_{d,geno} + \beta_{age} X_{d,age} + \beta_{sex} X_{d,sex} + \beta_{nUMI} \log(X_{i,nUMI}) + \beta_{MT} X_{i,MT} + \sum_{k=1}^{5} \beta_{gPC_k} X_{d,gPC_k} + \sum_{k=1}^{5} \beta_{ePC_k} X_{i,ePC_k} + \beta_{CV1} X_{i,CV1} + \beta_{GxCV1} X_{d,geno} X_{i,CV1} + (\phi_d \mid d) + (\kappa_b \mid b)$$

Then, we calculated a two-sided empirical p value for the gene by comparing the β_{GxCV1} estimated in the actual dataset to the null distribution composed of the β_{GxCV1} estimates from the 1,000 null datasets. We conducted these simulations for 12 genes, including eGenes with and without significant CV1-eQTL interactions.

Simulating differential expression

We selected genes with non-significant cell state and cell-state interaction terms in the PME model with CD4+ as the cell state of interest. To test robustness of the single-cell models to differential expression, we uniformly reduced the expression level of each gene in each cell to 50%, 20%, and 10% of baseline expression. For PME, we did this in $\log_2$-space, converted back to counts, and rounded to the nearest whole number. For LME, we reduced expression in log2(counts per 10,000) space. Then, we ran the single-cell Poisson model with cell-state interaction (cell state = CD4+ cells).

Clustering eQTLs

We selected cell-state-dependent eGenes (Wald p value for at least two CVs in multivariate model < 0.05/7/6511 = 1.1 x 10^{-6}). For each eGene, we extracted the beta estimate for each cell state interaction term from the Poisson model and multiplied them by the sign of the main genotype beta to standardize directions of effect, i.e., positive value means interaction amplifies baseline genotype effect, negative value means interaction dampens effect. For each gene, we scaled the betas across CVs, keeping the center at 0 and scaling the maximum absolute value to 1 or -1. Using Seurat, we built a shared nearest neighbor graph and used Louvain clustering with n.start = 20, n.iter = 20, and resolution = 3 to define ten clusters of eGenes[84].

We explored the potential biological significance of the clusters by measuring the enrichment of MSigDB Gene Ontology (C5) gene sets (n = 5,917). For each gene set, we used a Fisher's exact test to compare the proportion of eGenes in the cluster that overlapped with the gene set versus the proportion in other clusters that overlapped with the gene set.

Transcription factor binding motif enrichment

We used HOMER [v.4.8.3] to measure the enrichment of transcription factor binding motifs near eGenes associated with specific CVs[36]. First, we conducted a gene-level analysis. For each CV, we selected eGenes with significant state dependence and used HOMER's findMotifs function to search for transcription factor binding motifs of length 8 and 10 within +/-2kb of the transcription start site. Next, we conducted a variant-level analysis. For each CV, we selected the lead eQTL variants with significant state dependence, converted them to hg19 coordinates, and made a BED file containing the +/- 20 bp windows around these variants. We used HOMER's findMotifsGenome function to search for transcription factor binding motifs within these given windows.

CV GO term enrichment

For each CV, we selected the eGenes with state-dependent lead or secondary eQTLs in the multivariate model. Then, we measured the enrichment of lead and secondary interacting genes for each CV in the multivariate model separately (2 x 7 = 14 analyses) in MSigDB Gene Ontology (C5) gene sets (n = 5,917 from msigdbr R package) with a Fisher's exact test, as described above.

Cumulative eQTL interaction effect

The effect of each eQTL in each cell is the cumulation of the main genotype effect and all of the genotype x CV interactions. We calculated the overall effect for each eQTL in each cell by summing the genotype beta and the products of each CV score and the corresponding beta:

$$\beta_{total} = \beta_G + \sum_{k=1}^{7} \beta_{GxCV_k} X_{i,CV_k}$$

For interpretation in some analyses, we defined cluster-level betas by averaging cell-level betas for all cells assigned to that cluster in the previous study.

GWAS variant enrichment:

We downloaded the GWAS Catalog as of July 30, 2020, restricted to GWAS in European populations, and identified variants associated with each of 194 traits at $p < 5x10^{-8}$ and pruned with PLINK to remove variants with LD $r^2 > 0.2$[38,60]. We also constructed a set of background variants by pooling variants associated with any trait at $p < 5x10^{-8}$ and pruning with plink to remove variants with LD $r^2 > 0.2$.

For each memory-T cell eQTL, we identified all other variants with LD $r^2 \geq 0.5$ in both the 1000 Genomes Peruvians in Lima, Peru (PEL) and European (EUR) populations. We then matched these variants with variants from the GWAS Catalog for 194 traits and the background variant set. We calculated all enrichments with a two-sided Fisher test. To calculate memory-T-cell eQTL enrichments for specific traits, we compared the proportion of eQTL-colocalizing GWAS variants for each trait with the proportion of eQTL-colocalizing background variants. To calculate the enrichment of GWAS variants colocalizing with state-dependent eQTLs, we compared the proportion

of eQTL lead variants with significant cell-state interaction (LRT q < 0.05 from the model with 7 CVs) that colocalize with the background variant set compared to the proportion of eQTLs without significant cell-state interaction that colocalize.

We then used coloc (coloc.abf function in coloc R package) to conduct a Bayesian test of whether the eQTL and GWAS associations in each locus were driven by the same causal variant[85]. We prioritized 15 immune and non-immune traits for this deeper colocalization analysis: atopic dermatitis[86], ankylosing spondylitis87, asthma88, coronary artery disease[89], Crohn's disease[42], height[90], inflammatory bowel disease[42], lymphocyte count[90], multiple sclerosis[91], osteoporosis[92], rheumatoid arthritis[93], psoriasis[94], systemic lupus erythematosus[95], type 1 diabetes[96], and type 2 diabetes[97], and obtained summary statistics from the GWAS Catalog or UK Biobank (for height and lymphocyte count). We designated loci with significant colocalization as those with posterior probability of H_4 ("both traits are associated and share a single causal variant") > 0.5.

Fine-mapping memory-T cell eQTLs

For each locus (eGene), we used CAusal Variants Identification in Associated Regions (CAVIAR) software allowing only a single causal variant in each locus (-c 1) to estimate the probability that each variant in a +/- 250kb window around the transcription start site (TSS) is causal[45]. We ran CAVIAR on pseudobulk eQTL z scores for these variants and pairwise Pearson correlation coefficients between the variants (calculated with plink version v1.9b)[60].

For joint multi-ancestry analysis, we obtained raw data for naive CD4+ T cells (genotypes called from whole genome sequencing, and whole-transcriptome gene

expression from bulk RNA-seq) from BLUEPRINT. We used IMPUTE2 to impute genotypes at uncalled loci with 1000 Genomes Project Phase 3 dataset as a reference panel, and we removed variants with INFO scores < 0.9, MAF < 0.5, call rate < 95%, and Hardy-Weinberg p < 1e-05[30]. To align the two datasets, we lifted the imputed genotypes to GRCh38 with liftOver and matched variants on chromosome, position, reference, and alternate alleles. This produced a merged genotype dataset with a set of shared variants and 428 donors (259 from TBRU, 169 from BLUEPRINT).

The gene expression data obtained from BLUEPRINT were already normalized and batch-corrected. We inverse-normal transformed each gene so that its expression was normally distributed across donors and then conducted PEER normalization (correcting for donor age, sex, and top three genotype PCs, with K = 30 as recommended for this sample size by GTEx)[75]. We merged the matrix of PEER residuals from BLUEPRINT with the matrix of PEER residuals from TBRU (produced as described above)—matching on genes—and regressed out a dataset covariate in order to account for systematic differences between the bulk European BLUEPRINT data and the pseudobulk Peruvian TBRU data.

We then performed eQTL analysis on this final merged dataset with a linear model implemented in FastQTL to associate each gene's expression with variants within 1 MB of its TSS. We fine-mapped each locus with CAVIAR using z scores from the joint analysis, as described in the Peruvian dataset.

Enrichment of eQTLs in regulatory regions

We defined promoters as the region +/- 2kb from the transcription start site of each of the 6,511 significant eGenes based on the Cell Ranger 3.1.0 GTF. This annotation was binary.

We defined cell-state-specific regulatory regions with a probabilistic annotation of the genome by Inference and Modeling of Phenotype-related ACtive Transcription (IMPACT)[46]. First, we collected public T-bet (*TBX21*) ChIP-seq data for in CD4+ T_H1 cells from NCBI as a gold standard for CD4+ T_H1 regulatory elements[98]. We also previously aggregated 5,345 public epigenetic features from NCBI, ENCODE, and Roadmap spanning all possible cell types[99]. Then, we used IMPACT's logistic regression model to distinguish 1,000 T-bet bound sequence motifs from 10,000 unbound T-bet sequence motifs genome-wide based on epigenetic feature characterization. We used HOMER [v.4.8.3] to identify T-bet sequence motif matches as previously done[36,46]. We then characterized every nucleotide genome-wide using the same set of epigenetic features and estimated the probability (between 0 and 1) of a regulatory element important to the cell type.

For both the Peruvian and multi-ancestry analyses, we restricted loci to those that were also significant eQTLs in the Peruvian-only eQTL analysis. We computed enrichments in each locus containing a variant with posterior inclusion probability ≥ 0.5 and averaged across loci. To compute enrichments for the binary promoter annotation, we determined whether each variant in the locus overlapped with a promoter region (X = 0 if no overlap, X = 1 if overlap). Then, we calculated the enrichment across n variants in the locus as:

$$\sum_{i=1}^{n} \frac{E(PIP * X)}{E(PIP) * E(X)}$$

To compute enrichments for the probabilistic IMPACT T cell regulatory region annotations, we used the same strategy but X = the IMPACT score between 0 and 1 for each variant. We determined the significance of each enrichment by comparing the true enrichment score to a null distribution constructed by permuting the PIPs across variants in each locus 1,000 times and calculating an enrichment score. We determined the significance of the difference between the enrichments in interacting vs. non-interacting eGenes by comparing the true difference to a null distribution constructed by permuting interacting vs. non-interacting labels across eGenes and calculating an enrichment score. Both p values were computed with a one-sided comparison.

We also computed eQTL enrichment in ATAC-seq peaks from eight sorted T cell subsets published in Calderon, et al. 2019 (GSE118189): naive CD8+, naive CD4+ effector, naive CD4+ T_{reg}, central memory CD8+, effector memory CD8+, memory CD4+ effector, memory CD4+ Tr_{eg}, and gamma delta[48]. We downloaded peak counts files, normalized to counts per million within each sample, and for each T cell subset, averaged each peak's values across samples. We constructed a binary annotation in which peaks were considered open at a threshold of >5 CPM. To compute enrichments and determine significance, we used the same strategies described above for promoter enrichments.

Re-analysis of PBMC single-cell and genotyping data

We used a published single-cell dataset of PBMCs from an influenza A virus (IAV) exposure study[24]. The original study included pairs of mock-treated and IAV-exposed samples from each of 90 male donors. Methods for PBMC isolation and IAV

infection are detailed in the original study. Starting with the counts matrix, we first removed UMIs that mapped to 10 IAV genes (PB2, PB1, PA, HA, NP, NA, M2, M1, NEP, NS1). Then, we removed cells with < 500 genes expressed or > 10% mitochondrial UMIs, and used the 208,223 remaining high-quality cells for further analysis. We processed single-cell data first for mock-treated samples only, and then for all samples together. After QC there were 108,209 cells from mock-treated samples and 100,014 cells from IAV-exposed samples. In each analysis, we selected the top 300 most variable genes per sample based on variance-stabilized transformation and pooled them together. Then, we normalized the expression of all genes within each cell to log2(counts per 10,000), scaled variable genes to have mean = 0/variance = 1, and cosine (L2) normalized the scaled values. We used truncated PCA (irlba R package) to define 20 PCs and corrected donor and batch effects with Harmony. We produced two-dimensional embeddings for visualization with UMAP.

All donors were sequenced with low-pass (4x) whole-genome sequencing. Methods for genomic data processing, variant calling, and imputation are detailed in the original study. Starting with imputed genotypes for 89 donors passing QC in the original study, we followed the same QC procedures they described and set positions with GP < 0.9 to missing and then filtered out variants with missing call rate > 1%, minor allele frequency < 5%, and Hardy-Weinberg equilibrium p < 10-5. After this QC, 5,194,816 genetic variants remained genomewide. We selected 508,883 independent variants

using Plink (--indep-pairwise 50 5 0.2) and performed principal component analysis using the R package SNPRelate.

State-dependent eQTL analysis across five cell types in untreated PBMCs

First, we defined a set of PBMC eQTLs to test for state dependence through pseudobulk analysis. We removed lowly expressed genes, aggregated the mock-treated single cells into pseudobulk samples, and normalized to log2(counts per million) as described above for the memory T cell pseudobulk analysis. We inverse-normal transformed these values and used PEER normalization to regress out the effects of age, 5 genotype PCs (explaining 46.5, 9.47, 5.07, 4.50, and 2.63%, respectively, of the genetic variance captured by the top 20 PCs, **Supplementary Fig. 2c**), and up to 15 PEER factors based on published optimizations[33].

We conducted pseudobulk eQTL analysis with these residuals in a ±1MB window with FastQTL's permutation mode for all 22 autosomal chromosomes with default settings. We calculated q values for the lead SNP for each gene and selected eGenes

with q < 0.05. We then tested these eQTLs for interactions with either the first 6 batch-corrected PCs:

$$\boldsymbol{\log(E_i) = \theta + \beta_G X_{d,geno} + \beta_{age} X_{d,age} + \beta_{sex} X_{d,sex} + \beta_{nUMI} \log(X_{i,nUMI}) + \beta_{MT} X_{i,MT}}$$
$$\boldsymbol{+ \sum_{k=1}^{5} \beta_{gPC_k} X_{d,gPC_k} + \sum_{k=1}^{5} \beta_{ePC_k} X_{i,ePC_k} + \sum_{k=1}^{n} \beta_{PC_k} X_{i,PC_k}}$$
$$\boldsymbol{+ \sum_{k=1}^{n} \beta_{GxPC_k} X_{d,geno} X_{i,PC_k} + (\phi_d \mid d) + (\kappa_b \mid b)}$$

or each of five cell types (B cells, CD4+ T cells, CD8+ T cells, NK cells, monocytes) in a univariate single-cell PME interaction model:

$$\log(E_i) = \theta + \beta_G X_{d,geno} + \beta_{age} X_{d,age} + \beta_{sex} X_{d,sex} + \beta_{nUMI} \log(X_{i,nUMI}) + \beta_{MT} X_{i,MT}$$
$$+ \sum_{k=1}^{5} \beta_{gPC_k} X_{d,gPC_k} + \sum_{k=1}^{5} \beta_{ePC_k} X_{i,ePC_k} + \beta_{cell\ type} X_{i,cell\ type}$$
$$+ \beta_{Gxcell\ type} X_{d,geno} X_{i,cell\ type} + (\phi_d \mid d) + (\kappa_b \mid b)$$

For each, we compared the model to the null model (without the interaction term) and calculated an LRT p value, and used q values to determine significance of the interaction (q < 0.05).

eQTL interaction testing in mock-treated and IAV-exposed monocytes

Starting by selecting cells labeled in Randolph, et al. as “monocytes” or “infected monocytes” from all mock- and IAV-treated cells (n=24,783 cells total), we first used SCTransform to normalize and scale the expression of the top 3,000 variable genes[31,43]. Then, we ran truncated PCA (prcomp_irlba, from irlba R package) and corrected the top 10 PCs for donor, batch, and treatment effects with Harmony (HarmonyMatrix: default parameters, all thetas = 1, epsilon.cluster = -Inf, epsilon.harmony = -Inf, max.iter.cluster

= 10)[83]. We projected cells into a two-dimensional embedding for visualization with UMAP (umap, from uwot R package: default parameters, n_neighbors = 30L, min_dist = .1).

For trajectory analysis, we used DDRTree (R function: ncenter = 137, param.gamma = 10, maxIter = 20, tol = 1e-3, sigma = 0.0001)[59]. We fit a principal curve to the resulting low-dimensional embedding to calculate pseudotime for each cell (principal_curve from princurve R package)[60].

We conducted a pseudobulk eQTL analysis within the mock-treated monocytes as described above, and pooled the significant eQTLs with the significant eQTLs from the mock PBMC analysis described above (in total, 997 eGenes at q < 0.05). For the single-cell PME interaction model, we used the following PME model, implemented with the glmer function in the lme4 R package:

$$\log(E_i) = \theta + \beta_G X_{d,geno} + \beta_{age} X_{d,age} + \beta_{sex} X_{d,sex} + \beta_{nUMI} \log(X_{i,nUMI}) + \beta_{MT} X_{i,MT} + \sum_{k=1}^{5} \beta_{gPC_k} X_{d,gPC_k} + \sum_{k=1}^{5} \beta_{ePC_k} X_{i,ePC_k} + \beta_{Trajectory} X_{i,Trajectory} + \beta_{GxTrajectory} X_{d,geno} X_{i,Trajectory} + (\phi_d \mid d) + (\kappa_b \mid b)$$

We compared this model to the null model and calculated an LRT p value:

$$\log(E_i) = \theta + \beta_G X_{d,geno} + \beta_{age} X_{d,age} + \beta_{sex} X_{d,sex} + \beta_{nUMI} \log(X_{i,nUMI}) + \beta_{MT} X_{i,MT} + \sum_{k=1}^{5} \beta_{gPC_k} X_{d,gPC_k} + \sum_{k=1}^{5} \beta_{ePC_k} X_{i,ePC_k} + \beta_{Trajectory} X_{i,Trajectory} + (\phi_d \mid d) + (\kappa_b \mid b)$$

We considered eQTLs with q < .05 to be significant.

eQTL interactions with states projected from an inflamed colon T cell reference

We obtained single-cell UMI count matrices from Smillie, et al. 2019 (Single Cell Portal accession SCP259)[49]. From the immune cells, we selected cells that had been

annotated as T cells in the original study (n=73,084) and removed cells with more than 20% mitochondrial UMIs or fewer than 300 genes expressed (n=69,460 remaining). We selected the 200 most variable genes per donor based on variance stabilizing transformation, normalized the expression of all genes in each cell to log2(counts per 10,000), and scaled and L2 normalized variable genes, excluding cell cycle genes. We calculated 20 PCs with the prcomp_irlba function and built a reference with Symphony that corrected for donor batch effects. Then, we mapped the 500,089 cells from the blood memory T cell dataset (Nathan, et al. 2021 *Nat Imm*) to this reference with Symphony (symphony R package) to correct for donor and library preparation batch effects.

Next, we conducted a state-dependent eQTL analysis using the PME model with the memory T cells' projections onto individual PCs from the ulcerative colitis dataset (UC-PCs) as the cell states:

$$\log(E_i) = \theta + \beta_G X_{d,geno} + \beta_{age} X_{d,age} + \beta_{sex} X_{d,sex} + \beta_{nUMI} \log(X_{i,nUMI}) + \beta_{MT} X_{i,MT} + \sum_{k=1}^{5} \beta_{gPC_k} X_{d,gPC_k} + \sum_{k=1}^{5} \beta_{ePC_k} X_{i,ePC_k} + \beta_{UC-PC} X_{i,UC-PC} + \beta_{GxUC-PC} X_{d,geno} X_{i,UC-PC} + (\phi_d \mid d) + (\kappa_b \mid b)$$

We compared this to a null model without the interaction term, measured significance with an LRT, and corrected for multiple testing with q values (significance at $q < 0.05$).

Supplementary References

57 Stoeckius, M. *et al.* Simultaneous epitope and transcriptome measurement in single cells. *Nat Methods* **14**, 865-868, doi:10.1038/nmeth.4380 (2017).

58 Kang, H. M. *et al.* Multiplexed droplet single-cell RNA-sequencing using natural genetic variation. *Nat Biotechnol* **36**, 89-94, doi:10.1038/nbt.4042 (2018).

59 Korsunsky, I. *et al.* Fast, sensitive, and accurate integration of single cell data with Harmony. *Nat Methods*, doi:10.1101/461954 (2019).

60 Purcell, S. *et al.* PLINK: A Tool Set for Whole-Genome Association and Population-Based Linkage Analyses. *Am J Hum Genet* **81**, 559-575, doi:10.1086/519795 (2007).

61 Alexander, D. H., Novembre, J. & Lange, K. Fast model-based estimation of ancestry in unrelated individuals. *Genome Res* **19**, 1655-1664, doi:10.1101/gr.094052 (2009).

62 Buzkova, P., Lumley, T. & Rice, K. Permutation and Parametric Bootstrap Tests for Gene–Gene and Gene–Environment Interactions. *Ann Hum Genet* **75**, 36-45, doi:10.1111/j.1469-1809.2010.00572.x (2011).

63 Hu, Y., Xi, X., Yang, Q. & Zhang, X. SCeQTL: an R package for identifying eQTL from single-cell parallel sequencing data. *BMC Bioinformatics* **21**, 184, doi:10.1186/s12859-020-3534-6 (2020).

64 Suliman, S. *et al.* Peripheral Blood Mucosal-Associated Invariant T Cells in Tuberculosis Patients and Healthy Mycobacterium tuberculosis-Exposed Controls. *J Infect Dis* **222**, 995-1007, doi:10.1093/infdis/jiaa173 (2020).

65 Mao, Q., Wang, L., Goodison, S. & Sun, Y. Dimensionality Reduction via Graph Structure Learning. *The 21st ACM SIGKDD Conference on Knowledge Discovery and Data Mining (KDD'15)* (2015).

66 Hastie, T. & Stuetzle, W. Principal Curves. *J Am Stat Assoc* **84**, 502-516 (1989).

67 Luster, A. D., Unkeless, J. C. & Ravetch, J. V. Gamma-interferon transcriptionally regulates an early-response gene containing homology to platelet proteins. *Nature* **315**, 672-676, doi:10.1038/315672a0 (1985).

68 Peng, G. *et al.* Myeloid differentiation and susceptibility to HIV-1 are linked to APOBEC3 expression. *Blood* **110**, 393-400, doi:10.1182/blood-2006-10-051763 (2007).

69 Koning, F. A. *et al.* Defining APOBEC3 expression patterns in human tissues and hematopoietic cell subsets. *J Virol* **83**, 9474-9485, doi:10.1128/JVI.01089-09 (2009).

70 Kang, J. B. *et al.* Efficient and precise single-cell reference atlas mapping with Symphony. *Nat Commun* **12**, 5890, doi:10.1038/s41467-021-25957-x (2021).

71 Smillie, C. S. *et al.* Intra- and Inter-cellular Rewiring of the Human Colon during Ulcerative Colitis. *Cell* **178**, 714-730 e722, doi:10.1016/j.cell.2019.06.029 (2019).

72 Becerra, M. C. et al. Transmissibility and potential for disease progression of drug resistant Mycobacterium tuberculosis: prospective cohort study. BMJ 367, l5894, doi:10.1136/bmj.l5894 (2019).

73 O'Connell, J. et al. A general approach for haplotype phasing across the full spectrum of relatedness. PLoS Genet 10, e1004234, doi:10.1371/journal.pgen.1004234 (2014).
74 Howie, B. N., Donnelly, P. & Marchini, J. A Flexible and Accurate Genotype Imputation Method for the Next Generation of Genome-Wide Association Studies. PLoS Genet 5, e1000529, doi:10.1371/journal.pgen.1000529 (2009).
75 Stegle, O., Parts, L., M., P., Winn, J. & Durbin, R. Using probabilistic estimation of expression residuals (PEER) to obtain increased power and interpretability of gene expression analyses. Nat Protoc 7, 500-507, doi:10.1038/nprot.2011.457 (2012).
76 Ongen, H., Buil, A., Brown, A. A., Dermitzakis, E. T. & Delaneau, O. Fast and efficient QTL mapper for thousands of molecular phenotypes. Bioinformatics 32, 1479-1485, doi:10.1093/bioinformatics/btv722 (2016).
77 Storey, J. D. & Tibshirani, R. Statistical significance for genomewide studies. Proc Natl Acad Sci U S A 100, 9440-9445, doi:10.1073/pnas.1530509100 (2003).
78 Gonzalez, I., Déjean, S., Martin, P. G. P. & Baccini, A. CCA: An R Package to Extend Canonical Correlation Analysis. J of Stat Soft 23 (2007).
79 McInnes, L. & Healy, J. UMAP: Uniform Manifold Approximation and Projection for Dimension Reduction. arXiv, 1802.03426 (2018).
80 Subramanian, A. et al. Gene set enrichment analysis: A knowledge-based approach for interpreting genome-wide expression profiles. PNAS 102, 15545-15550, doi:10.1073/pnas.0506580102 (2005).
81 Korotkevich, G., Sukhov, V. & Sergushichev, A. Fast gene set enrichment analysis. bioRxiv, doi:10.1101/060012 (2019).
82 Gutierrez-Arcelus, M. *et al.* Lymphocyte innateness defined by transcriptional states reflects a balance between proliferation and effector functions. *Nat Commun* **10**, 687, doi:10.1038/s41467-019-08604-4 (2019).
83 Bates, D., Mächler, M., Bolker, B. & Walker, S. Fitting Linear Mixed-Effects Models Using lme4. J Stat Softw 67, 1-48, doi:10.18637/jss.v067.i01 (2015).
84 Stuart, T. et al. Comprehensive integration of single cell data. Cell 177, 1888-1902, doi:10.1016/j.cell.2019.05.031 (2019).
85 Giambartolomei, C. et al. Bayesian test for colocalisation between pairs of genetic association studies using summary statistics. PLoS Genet 10, e1004383 (2014).
86 Paternoster, L. et al. Multi-ancestry genome-wide association study of 21,000 cases and 95,000 controls identifies new risk loci for atopic dermatitis. Nat Genet 47, 1449-1456, doi:10.1038/ng.3424 (2015).
87 International Genetics of Ankylosing Spondylitis, C. et al. Identification of multiple risk variants for ankylosing spondylitis through high-density genotyping of immune-related loci. Nat Genet 45, 730-738, doi:10.1038/ng.2667 (2013).
88 Demenais, F. et al. Multiancestry association study identifies new asthma risk loci that colocalize with immune-cell enhancer marks. Nat Genet 50, 42-53, doi:10.1038/s41588-017-0014-7 (2018).

89 van der Harst, P. & Verweij, N. Identification of 64 Novel Genetic Loci Provides an Expanded View on the Genetic Architecture of Coronary Artery Disease. Circ Res 122, 433-443, doi:10.1161/CIRCRESAHA.117.312086 (2018).
90 Bycroft, C. *et al.* The UK Biobank resource with deep phenotyping and genomic data. Nature 562, 203-209, doi:10.1038/s41586-018-0579-z (2018).
91 International Multiple Sclerosis Genetics, C. et al. Analysis of immune-related loci identifies 48 new susceptibility variants for multiple sclerosis. Nat Genet 45, 1353-1360, doi:10.1038/ng.2770 (2013).
92 Morris, J. A. et al. An atlas of genetic influences on osteoporosis in humans and mice. Nat Genet 51, 258-266, doi:10.1038/s41588-018-0302-x (2019).
93 Ishigaki, K. et al. Trans-ancestry genome-wide association study identifies novel genetic mechanisms in rheumatoid arthritis. medRxiv, doi:10.1101/2021.12.01.21267132 (2021).
94 Tsoi, L. C. et al. Identification of 15 new psoriasis susceptibility loci highlights the role of innate immunity. Nat Genet 44, 1341-1348, doi:10.1038/ng.2467 (2012).
95 Bentham, J. et al. Genetic association analyses implicate aberrant regulation of innate and adaptive immunity genes in the pathogenesis of systemic lupus erythematosus. Nat Genet 47, 1457-1464, doi:10.1038/ng.3434 (2015).
96 Onengut-Gumuscu, S. et al. Fine mapping of type 1 diabetes susceptibility loci and evidence for colocalization of causal variants with lymphoid gene enhancers. Nat Genet 47, 381-386, doi:10.1038/ng.3245 (2015).
97 Xue, A. et al. Genome-wide association analyses identify 143 risk variants and putative regulatory mechanisms for type 2 diabetes. Nat Commun 9, 2941, doi:10.1038/s41467-018-04951-w (2018).
98 Kanhere, A. et al. T-bet and GATA3 orchestrate Th1 and Th2 differentiation through lineage-specific targeting of distal regulatory elements Nat Commun 3, 1268, doi:10.1038/ncomms2260 (2012).
99 Amariuta, T. et al. Improving the trans-ancestry portability of polygenic risk scores by prioritizing variants in predicted cell-type-specific regulatory elements. Nat Genet 52, 1346–1354, doi:10.1038/s41588-020-00740-8 (2020).

Supplementary Figures

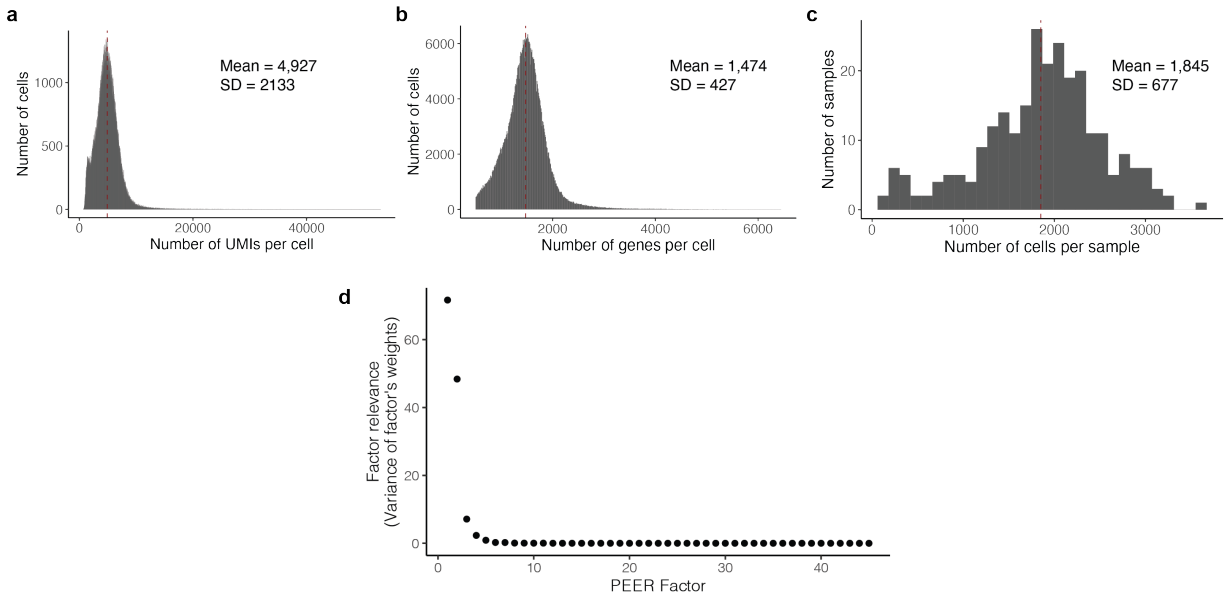

Supplementary Figure 1. Single-cell data quality and normalization. a, Histogram of 500,089 cells by number of UMIs and **b,** number of genes. **c,** Histogram of 259 samples by number of cells. Red dotted lines indicate the mean of each measurement. **d**, PEER factor relevance. Each dot represents the alpha for each factor.

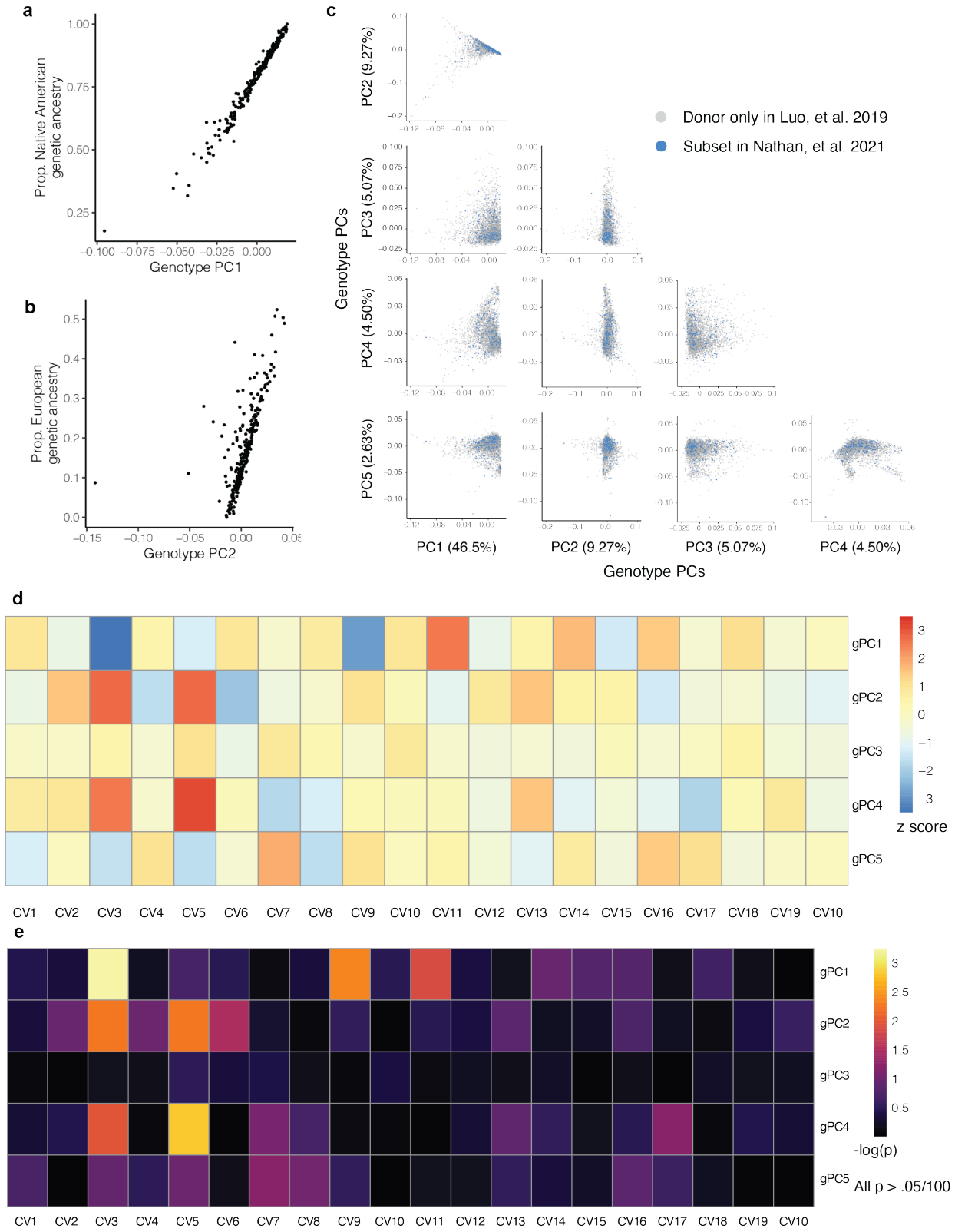

Supplementary Figure 2: Genetic data structure. a, Donors plotted by proportion of Native American genetic ancestry compared to genotype PC1 score or **b,** proportion of

European genetic ancestry compared to genotype PC2. **c,** Donors plotted according to scores on pairs of genotype PCs. Gray dots are from the original GWAS (n=4002), blue dots are from the single-cell study (n = 259). **d**, Heatmap of beta Wald z scores from multivariate linear mixed effects model of each CV's scores regressed on five genotype PCs, with a random effect for donor. **e**, Heatmap of -log(p) for betas from the same multivariate linear mixed effects model.

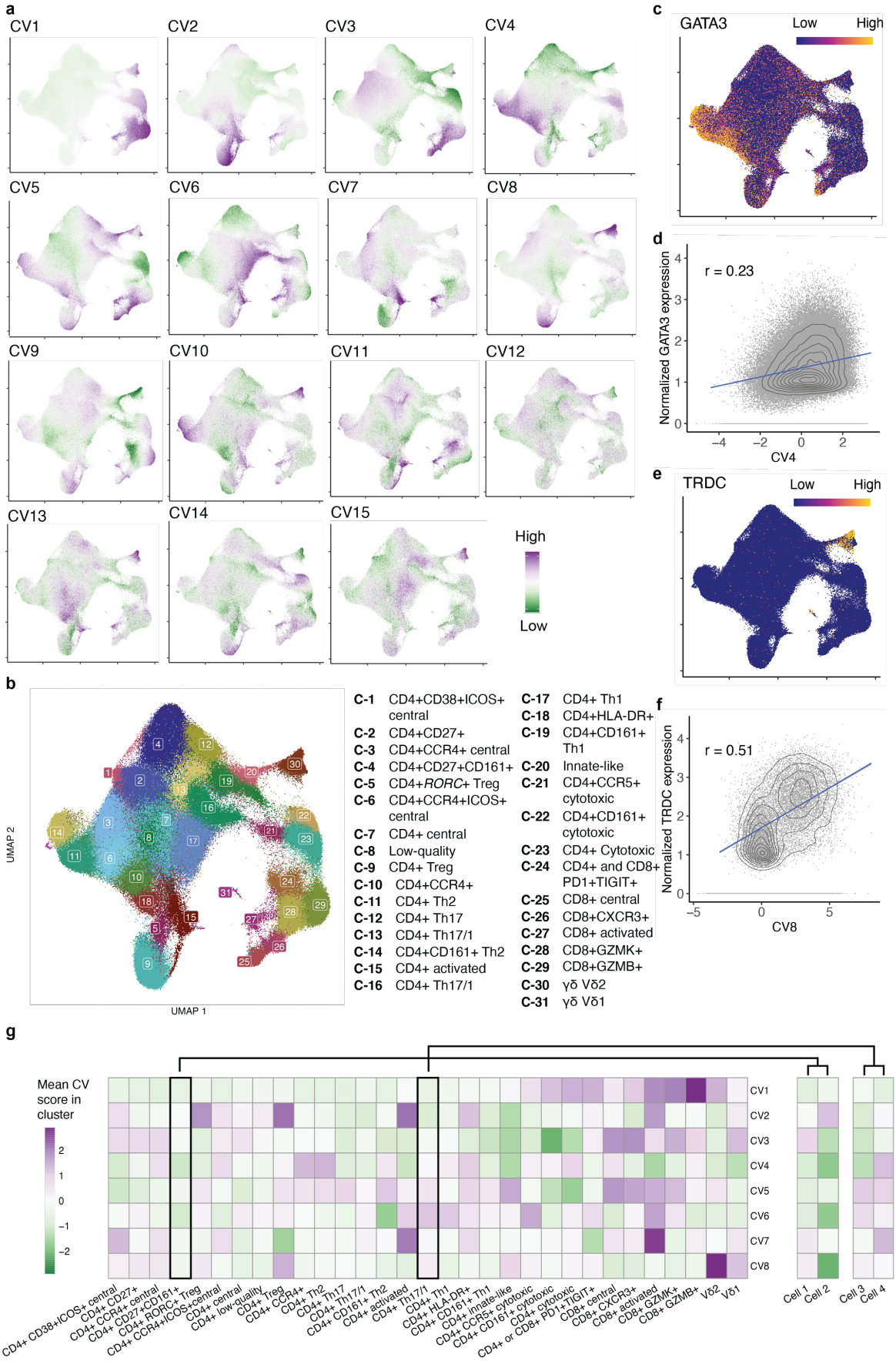
a
CV1
CV2
CV3
CV4
CV5
CV6
CV7
CV8
CV9
CV10
CV11
CV12
CV13
CV14
CV15
High
Low
c
GATA3
Low
High
d
r = 0.23
Normalized GATA3 expression
CV4
e
TRDC
Low
High
b
UMAP 2
UMAP 1
C-1 CD4+CD38+ICOS+ central
C-2 CD4+CD27+
C-3 CD4+CCR4+ central
C-4 CD4+CD27+CD161+
C-5 CD4+RORC+ Treg
C-6 CD4+CCR4+ICOS+ central
C-7 CD4+ central
C-8 Low-quality
C-9 CD4+ Treg
C-10 CD4+CCR4+
C-11 CD4+ Th2
C-12 CD4+ Th17
C-13 CD4+ Th17/1
C-14 CD4+CD161+ Th2
C-15 CD4+ activated
C-16 CD4+ Th17/1
C-17 CD4+ Th1
C-18 CD4+HLA-DR+
C-19 CD4+CD161+ Th1
C-20 Innate-like
C-21 CD4+CCR5+ cytotoxic
C-22 CD4+CD161+ cytotoxic
C-23 CD4+ Cytotoxic
C-24 CD4+ and CD8+ PD1+TIGIT+
C-25 CD8+ central
C-26 CD8+CXCR3+
C-27 CD8+ activated
C-28 CD8+GZMK+
C-29 CD8+GZMB+
C-30 γδ Vδ2
C-31 γδ Vδ1
f
r = 0.51
Normalized TRDC expression
CV8
g
Mean CV score in cluster
CV1
CV2
CV3
CV4
CV5
CV6
CV7
CV8
Cell 1
Cell 2
Cell 3
Cell 4
CD4+ CD38+ICOS+ central
CD4+ CD27+
CD4+ CCR4+ central
CD4+ CD27+CD161+
CD4+ CD4+RORC+ Treg
CD4+ CCR4+ICOS+central
CD4+ central
CD4+ low-quality
CD4+ Treg
CD4+ CCR4+
CD4+ Th2
CD4+ Th17
CD4+ Th17/1
CD4+ CD161+ Th2
CD4+ activated
CD4+ Th17/1
CD4+ Th1
CD4+ HLA-DR+
CD4+ CD161+ Th1
CD4+ innate-like
CD4+ CCR5+ cytotoxic
CD4+ CD161+ cytotoxic
CD4+ cytotoxic
CD4+ or CD8+ PD1+TIGIT+
CD8+ central
CD8+ CXCR3+
CD8+ activated
CD8+ GZMK+
CD8+ GZMB+
Vδ2
Vδ1

Supplementary Figure 3. Continuous canonical variates (CVs) capture single-cell heterogeneity. a, UMAP of memory T cells (n = 500,089) colored by score along each of the top 15 CVs from CCA-based integration of mRNA and protein expression in Nathan, et al. **b,** UMAP of 31 memory T cell clusters defined with Louvain clustering in Nathan, et al. **c** and **e,** UMAP of memory T cells colored by normalized expression (log2(UMI counts per 10,000)) for *GATA3* and *TRDC*. **d** and **f,** Cells plotted based on normalized expression of *GATA3* and CV4 score or *TRDC* and CV8 score. For cells with non-zero expression, blue line represents linear best-fit line, contours represent density of cells, and r is the Pearson correlation coefficient. **g,** Heatmap colored by average score for each CV (1-8) among cells in each cluster. Separate columns on the right show CV scores for two cells each from two clusters. Colors range from low (green) to high (purple).

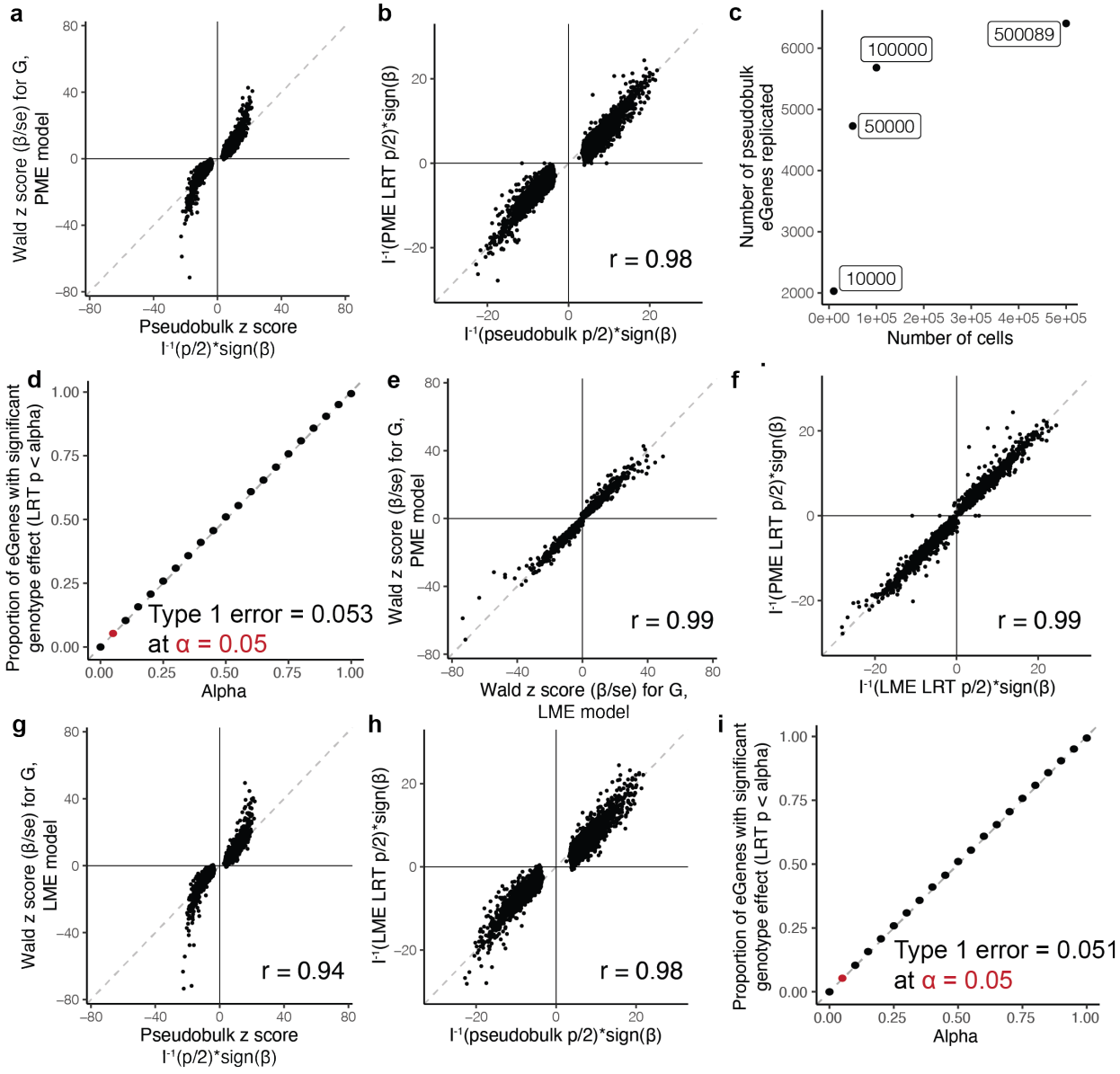

Supplementary Figure 4. Comparing PME and LME models for single-cell eQTL analysis. a and **g,** Pseudobulk-significant eGenes (n = 6,511) plotted based on z score from **a,** PME or **g,** LME single-cell model and pseudobulk model. Dashed line represents the identity line. **b** and **h,** Quantile-quantile plot of pseudobulk-significant eGenes plotted based on -log10 p value of genotype beta from **b,** PME or **h,** LME model with permuted genotypes and uniformly distributed quantiles. **c,** Number of pseudobulk eGenes replicated when downsampling cells. **d** and **i**, Type 1 error is calculated for **d,** PME and **i,** LME as the proportion of eGenes with p < 0.05 with permuted genotypes. **e** and **f,** Pseudobulk-significant eGenes plotted based on **e,** Wald z score or **f,** LRT-based statistic from PME and LME single-cell model. r was calculated as a Pearson correlation coefficient.

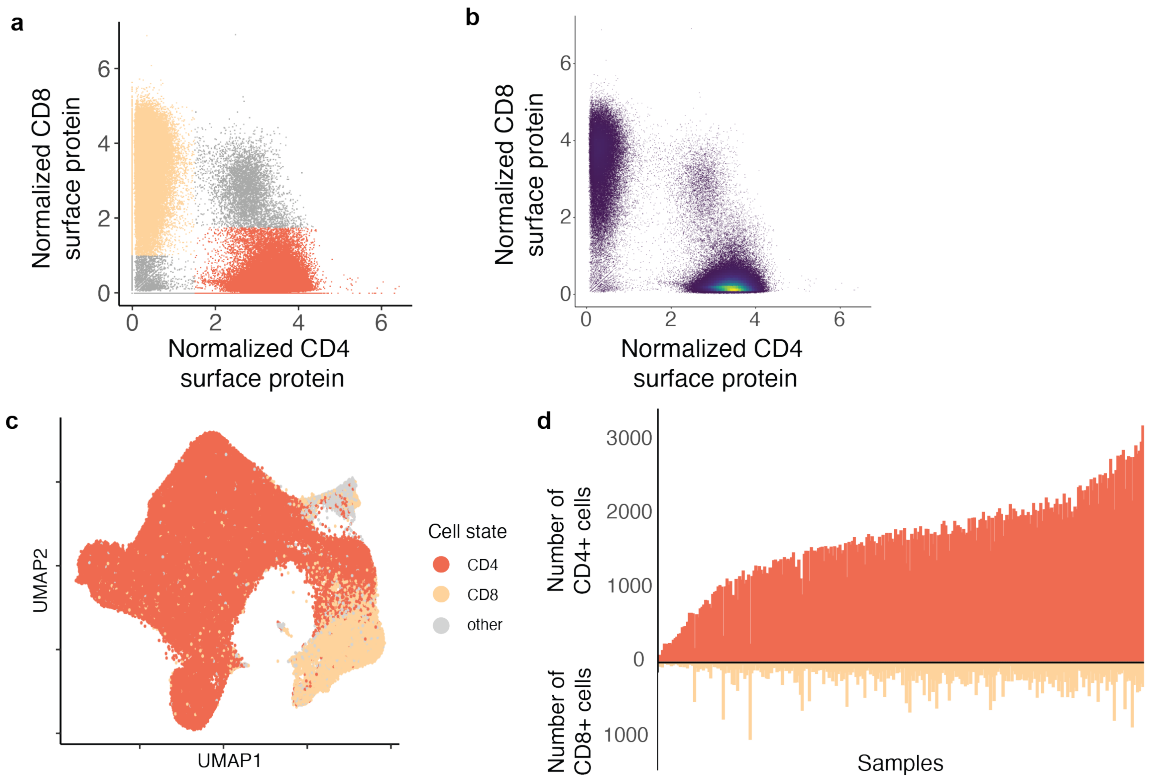

Supplementary Figure 5. Modeling discrete CD4+ and CD8+ cell states. A, Cells plotted by CLR-normalized CD8 and CD4 protein expression. Orange cells are CD4+CD8- and beige cells are CD4-CD8+ and in **b,** cells are colored by density. **c,** UMAP of 500,089 memory T cells colored by CD4+CD8- (orange) and CD4-CD8+ (beige). **d,** Bar graph of number of CD4+CD8- cells (top) and CD4-CD8+ cells (bottom) per sample (n = 259).

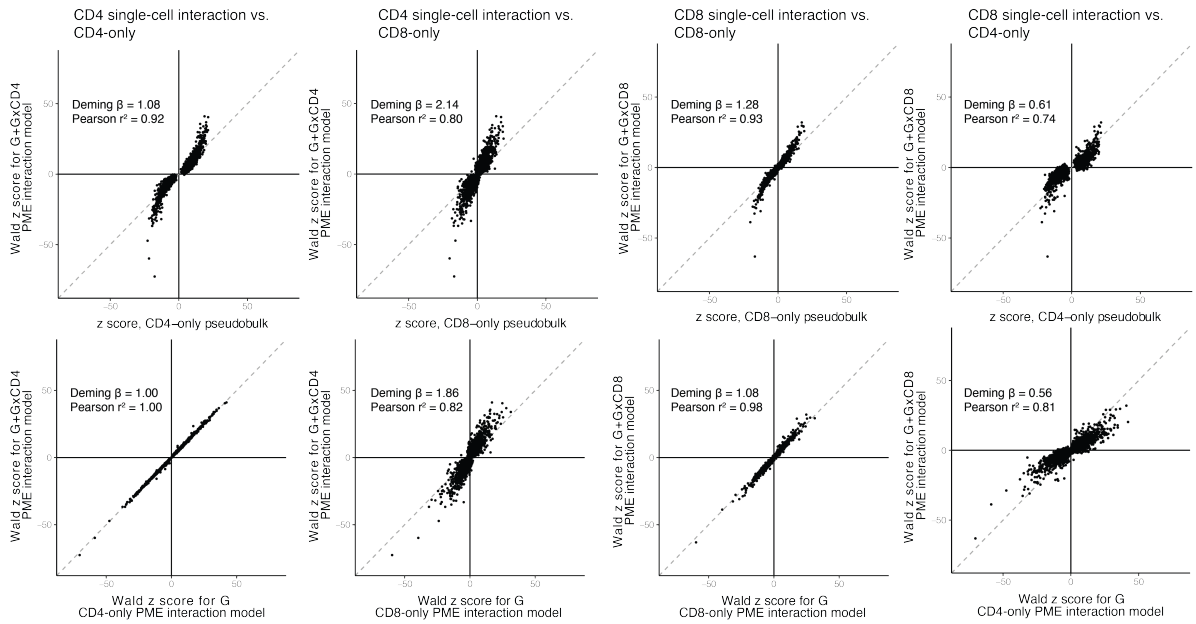

		CD4-only		CD8-only	
		pseudobulk	**single-cell**	**pseudobulk**	**single-cell**
CD4 sc-interaction		0.92	1.00	0.80	0.82
CD8 sc-interaction		0.74	0.81	0.93	0.98

Supplementary Figure 6: Cross-comparisons of eQTLs between lineages and statistical models. We compared CD4+ and CD8+ dependent effects estimated from the interaction model with the effects measured in the same and opposite lineages with non-interaction models, i.e., pseudobulk or single-cell eQTL models of gated CD4+ or CD8+ memory T cells. In the top row of plots, each dot is an eGene plotted according to its Wald z score in the interaction model and its LRT-based statistic (l^{-1}(LRT p/2)*sign(beta)) from pseudobulk. In the bottom row of plots, each dot is an eGene plotted according to its Wald z score in the interaction model and in the single-lineage (non-interaction) single-cell model. Deming regression betas and Pearson r^2 values are noted in the plots and the table below.

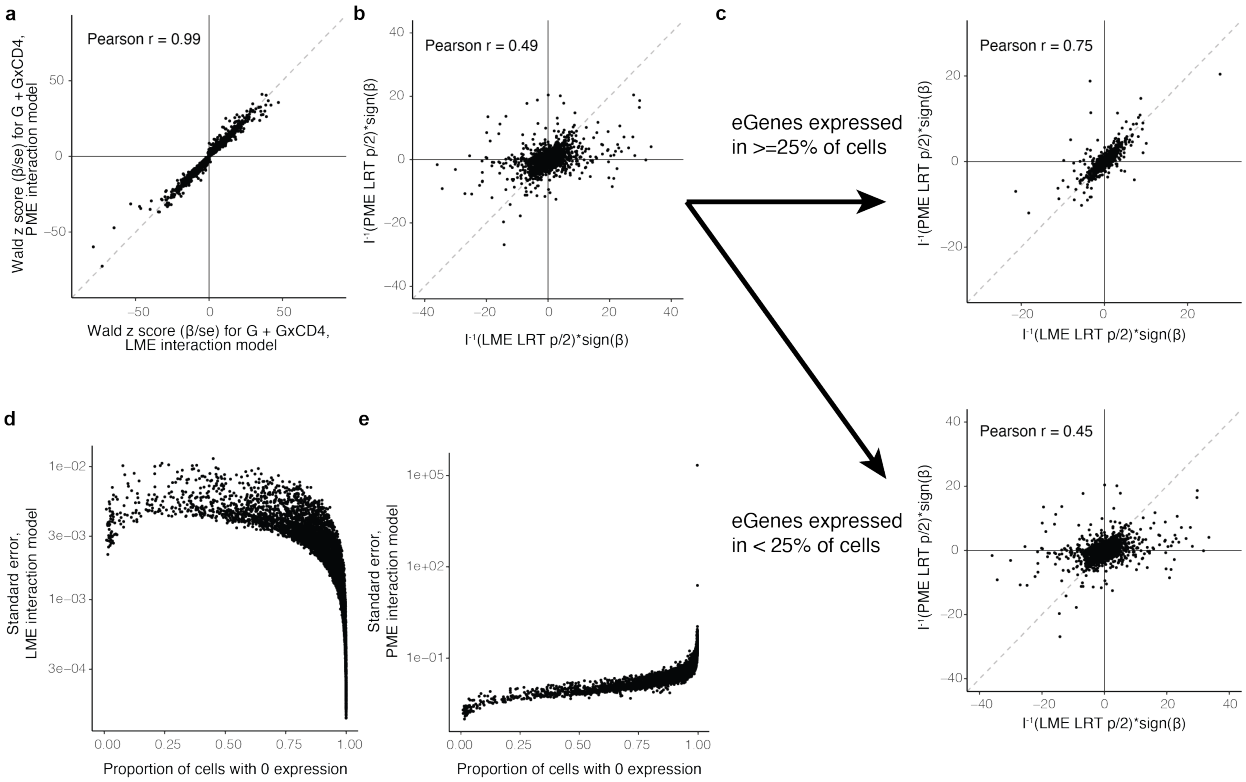

Supplementary Figure 7: Comparison of PME and LME interaction estimates. **a,** Comparison of Wald z scores for the GxCD4 term in PME and LME interaction models. In all plots, each point represents an eGene and the gray dashed line is the identity line. **b,** Comparison of LRT-based statistics (I^{-1}(LRT p/2)*sign(beta)) representing the significance of GxCD4 interaction in PME and LME models. **c,** Comparison from **(b)** subsetted by eGenes' sparsity. **d,** Standard error of the GxCD4 interaction estimate for each eGene, plotted against the gene's sparsity, from the LME and **e,** PME models.

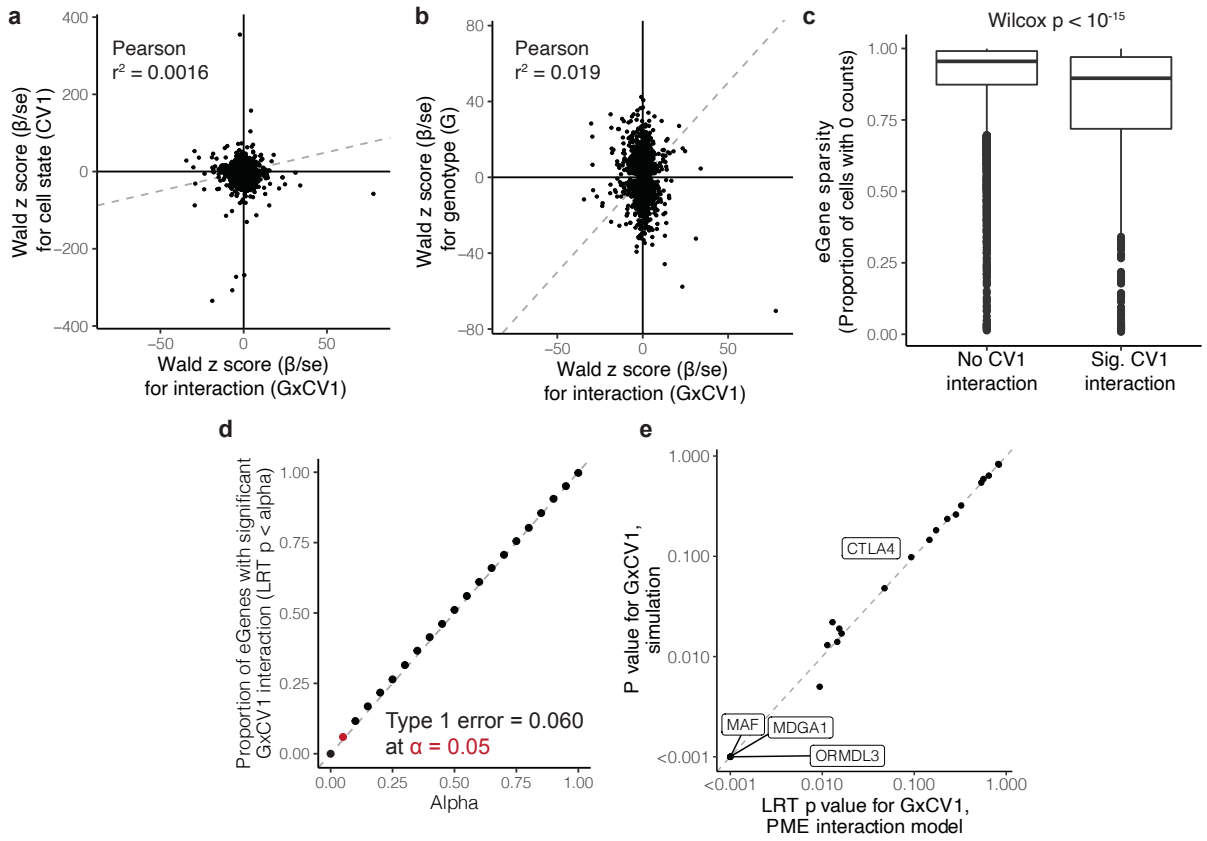

Supplementary Figure 8. Calibration of the PME interaction model. Dot plot of memory-T-cell eGenes (n = 6,511) based on z score for **a,** cell state beta (β_{CV1}) or **b,** genotype (β_G) and z score for cell state interaction beta (β_{GxCV1}) in PME model. **c,** Box plot of sparsity of eGenes with and without significant CV1 interactions (q < 0.05). Each point represents a gene. Box plots show median (horizontal bar), 25th and 75th percentiles (lower and upper bounds of the box, respectively) and 1.5 times the IQR (or minimum/maximum values if they fall within that range; end of whiskers). P value is from a two-sided Wilcoxon rank-sum test (n_{int}=1,094 genes, n_{no}=5,417). **d,** Proportion of eGenes with significant β_{GxCV1} under genotype permutation. Each dot represents the proportion significant at the given alpha threshold. **e,** Comparison of simulation-based empirical p value and LRT p value for the GxCV1 interaction effect on 12 genes. Each dot represents one gene, and genes discussed elsewhere in this paper are labeled.

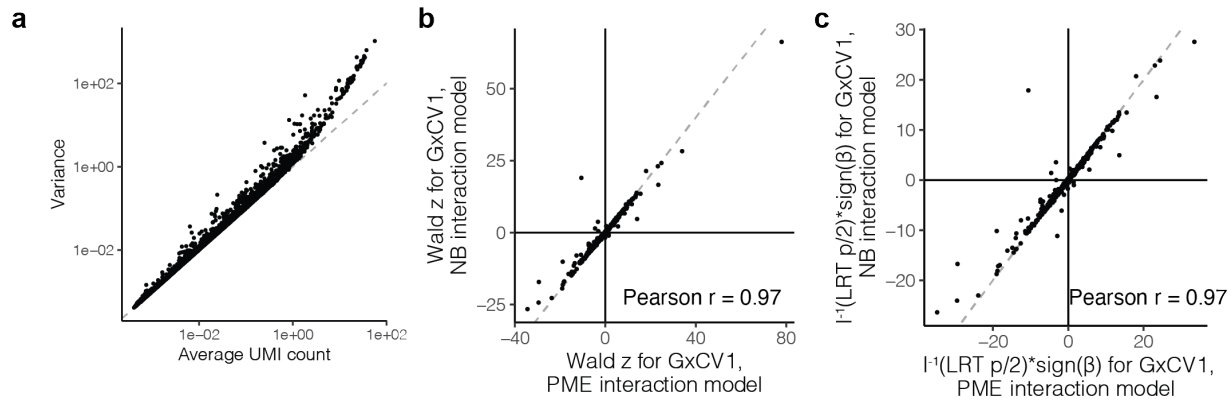

Supplementary Figure 9: Comparing Poisson and negative binomial models. a, Plot of genes' dispersion. In all plots, each point represents one of the pseudobulk-significant eGenes (n=6,511), here plotted based on its variance and mean UMI count across all 500,089 cells. In all plots, the gray dashed line is the identity line. **b**, Comparison of Wald z scores for the GxCV1 interaction term from negative binomial and Poisson models. **c**, Comparison of LRT-based statistic for significance of variance explained by the model with GxCV1 interaction compared to the null model without that term.

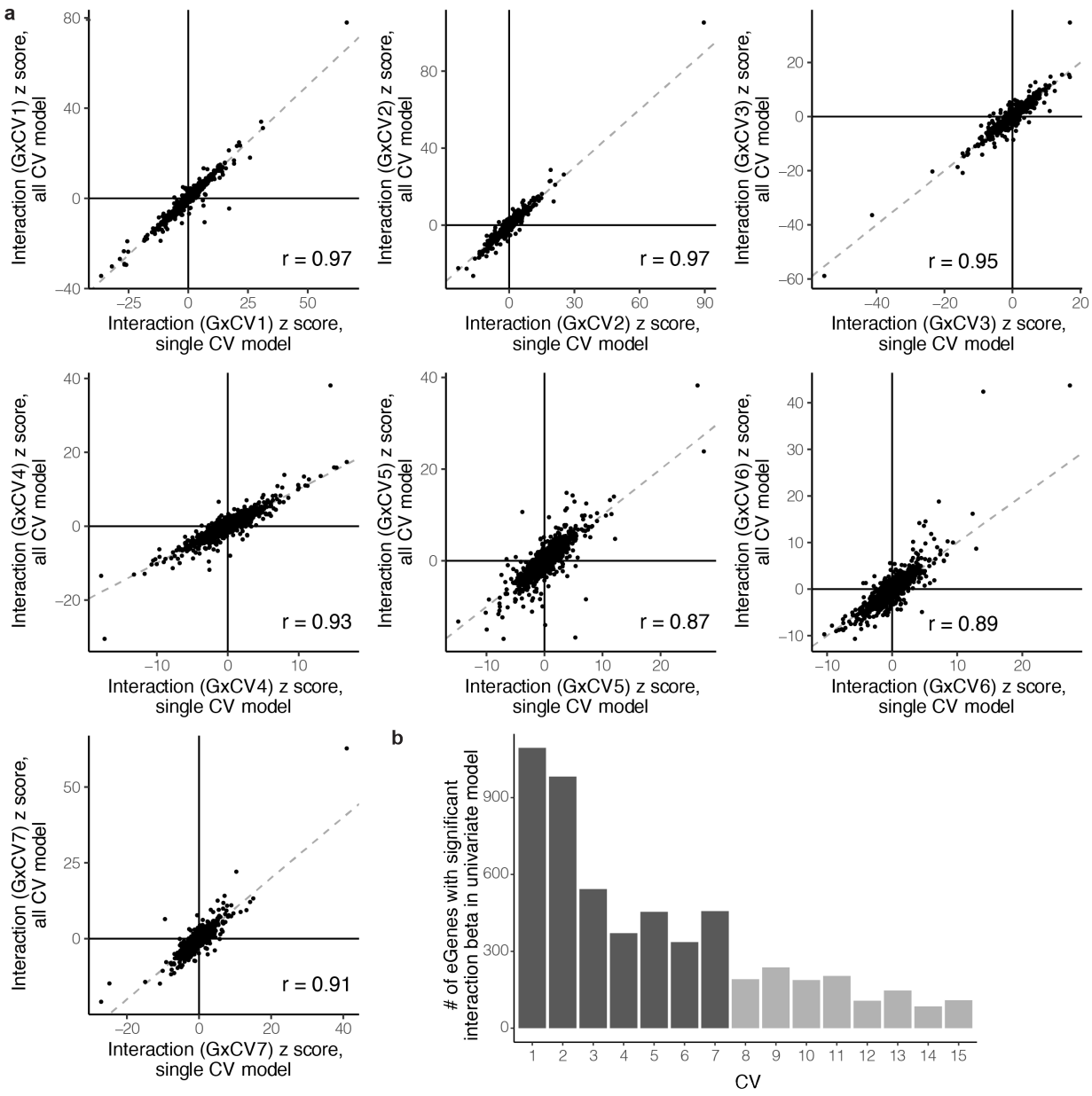

Supplementary Figure 10. Concordance of cell-state-dependent eQTL interactions from multivariate and univariate models. a, Dot plots of interaction z scores for each CV from multivariate model with 7 CVs and univariate model with one CV. Dashed line represents the identity line. r is calculated as the Pearson correlation coefficient. **b,** Number of eGenes with significant interaction with each CV in a corresponding univariate PME model.

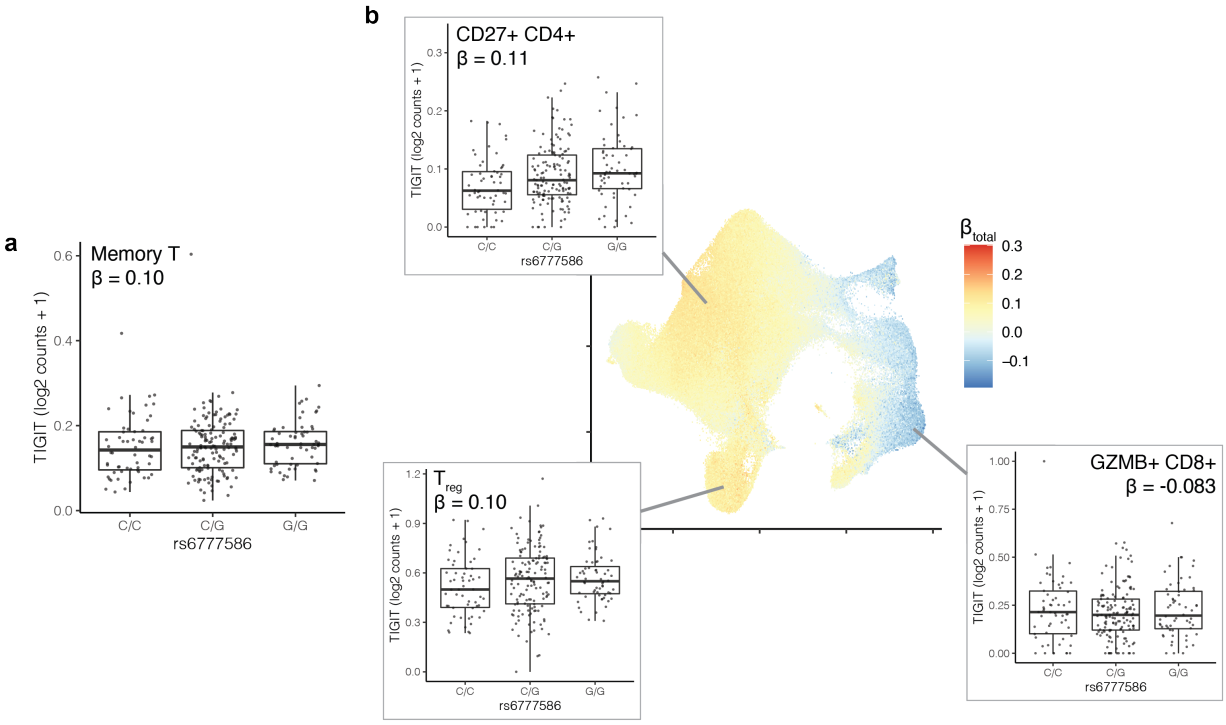

Supplementary Figure 11. State-dependence of a non-pseudobulk-significant eQTL. a, Box plot of rs6777586 eQTL for TIGIT across all memory T cells. **b,** UMAP of total effect size of eQTL at rs6777586 for *TIGIT*. In the UMAP, each cell is colored by its β_{total}, scaled to be centered on β_G with max (red) and min (blue) determined by the most extreme absolute β_{total} for that eQTL in any cell. For all box plots, each point represents the average log2(UMI counts + 1) across all cells in the indicated cluster in a donor (n = 259), grouped by genotype. Box plots show median (horizontal bar), 25th and 75th percentiles (lower and upper bounds of the box, respectively) and 1.5 times the IQR (or minimum/maximum values if they fall within that range; end of whiskers). Beta values are the average β_{total} for all cells in the cluster.

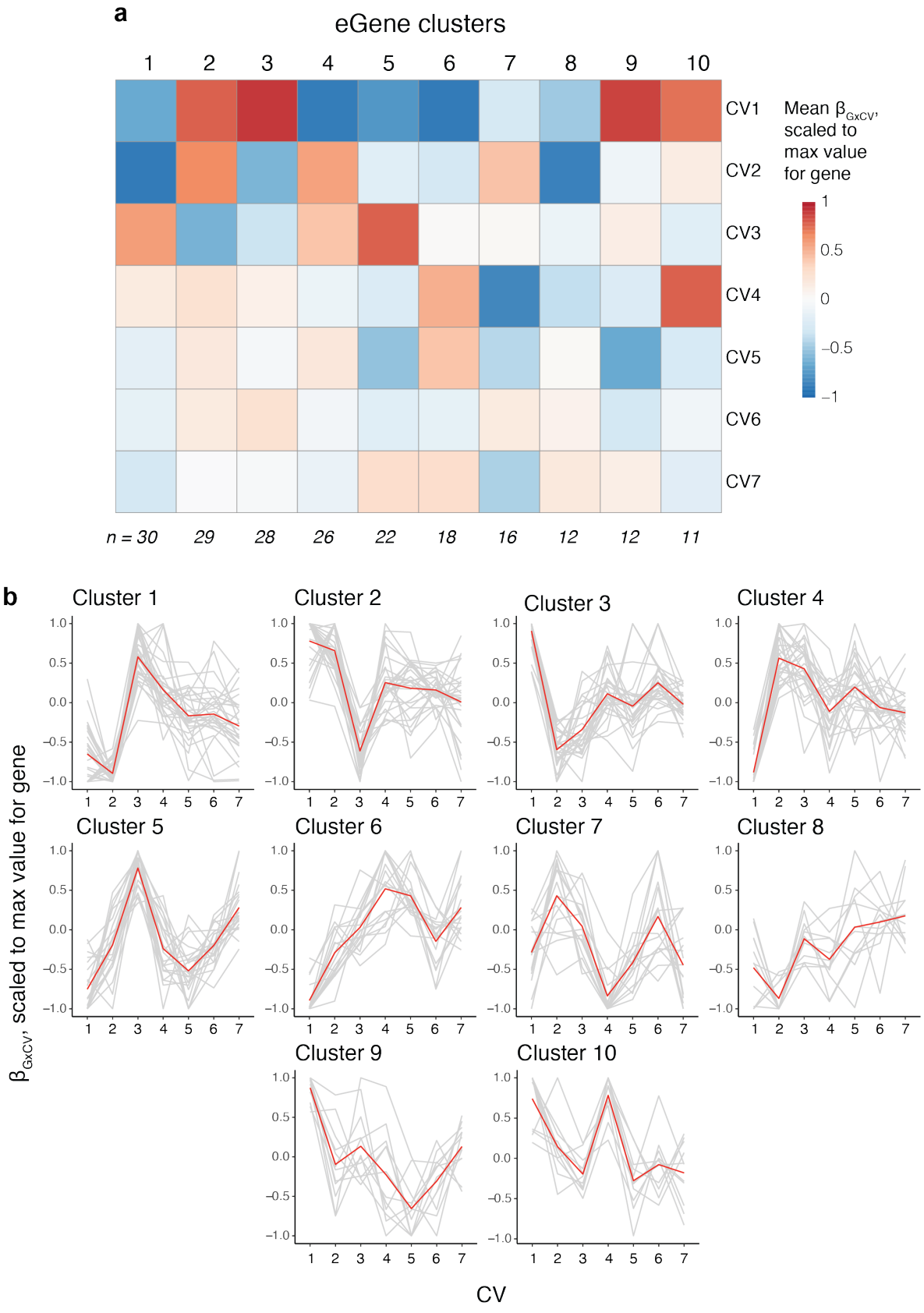
a
eGene clusters
1
2
3
4
5
6
7
8
9
10
CV1
CV2
CV3
CV4
CV5
CV6
CV7
Mean βGxCV, scaled to max value for gene
1
0.5
0
−0.5
−1
n = 30
29
28
26
22
18
16
12
12
11
b
Cluster 1
Cluster 2
Cluster 3
Cluster 4
Cluster 5
Cluster 6
Cluster 7
Cluster 8
Cluster 9
Cluster 10
βGxCV, scaled to max value for gene
CV

Supplementary Figure 12. Clustering eGenes based on CV interactions. a, Heatmap colored by average scaled interaction beta for each CV in the multivariate PME model, averaged across eGenes in each cluster. Clusters were defined through Louvain clustering on seven scaled betas calculated for 204 eGenes (at least one β_{GxCV} with Wald $p < .05/7/6511 = 1.10x10^{-6}$). Betas were scaled with respect to maximum interaction beta for each gene, and signs are relative to the main genotype effect. Colors are scaled from dampening the effect (blue) to amplifying the main effect (red). **b,** Line plots of scaled CV interaction betas for eGenes in each cluster. Each gray line represents one eGene and connects points corresponding to its scaled interaction beta for each CV. The red mean line connects points corresponding to the mean scaled interaction beta for each CV in each cluster.

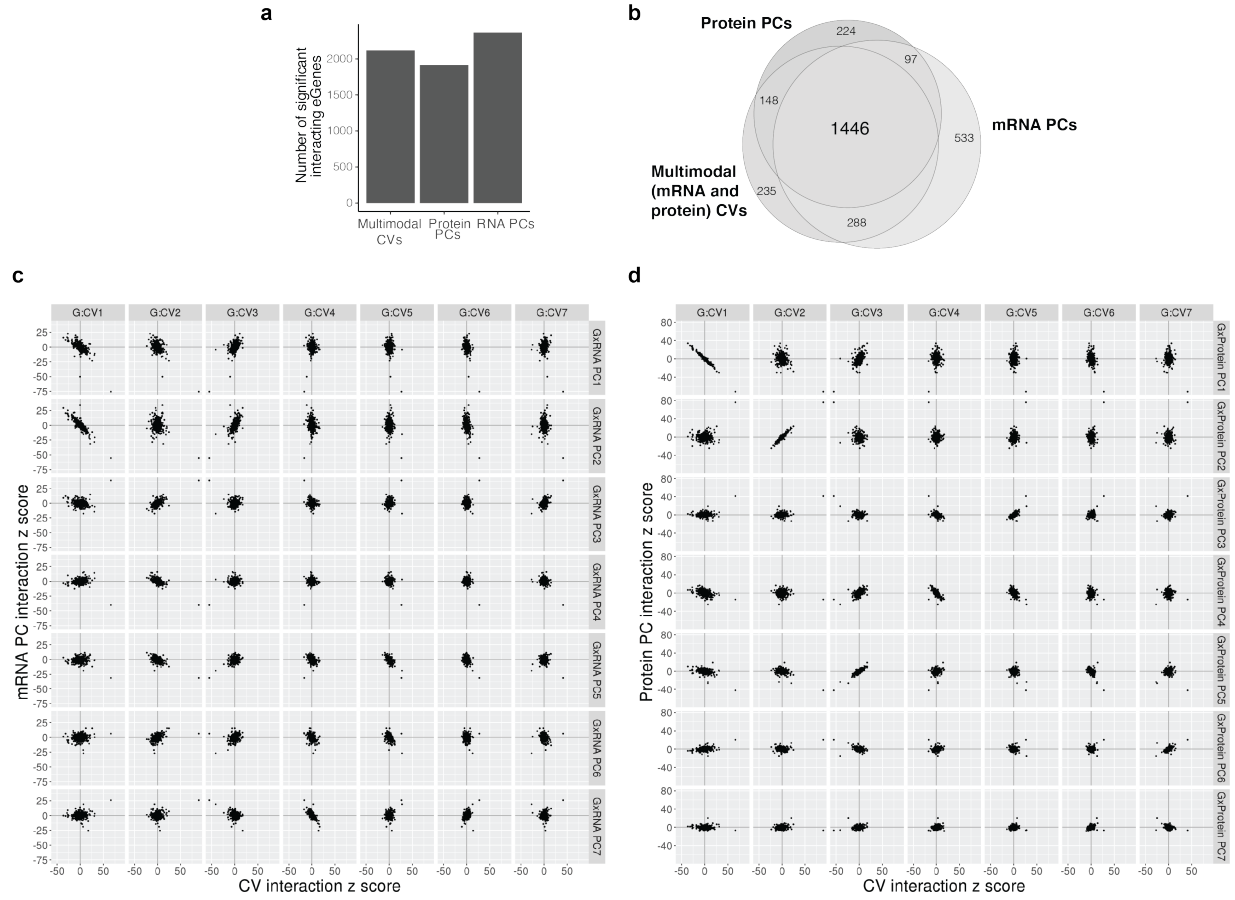

Supplementary Figure 13: eQTL interactions with unimodal PCs. **a,** Bar plot of the number of eGenes interacting with the top seven multimodal CVs, protein PCs, or mRNA PCs in multivariate models (significant at $q < 0.05$). **b,** Venn diagram of overlapping state-dependent eGenes from multivariate eQTL interaction models with the top seven multimodal CVs, protein PCs, or mRNA PCs. **c**, Concordance of Wald z scores for eQTL interaction terms between pairs of CVs and mRNA PCs (e.g., comparing z scores for GxCVx and GxmRNA PCx) or **d,** between pairs of CVs and protein PCs.

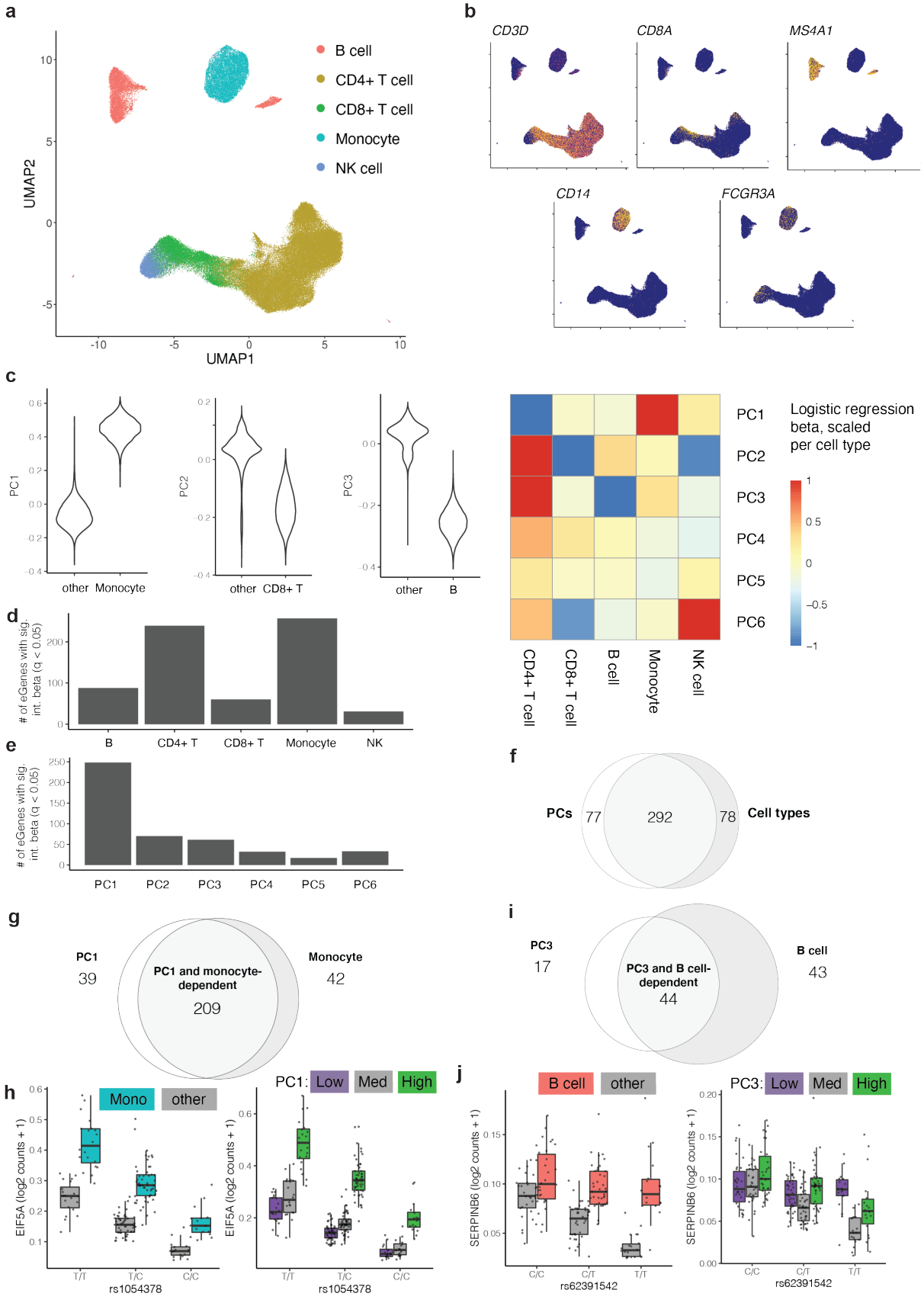
a
B cell
CD4+ T cell
CD8+ T cell
Monocyte
NK cell
UMAP2
UMAP1
b
CD3D
CD8A
MS4A1
CD14
FCGR3A
c
PC1
PC2
PC3
other Monocyte
other CD8+ T
other B
Logistic regression beta, scaled per cell type
PC1
PC2
PC3
PC4
PC5
PC6
CD4+ T cell
CD8+ T cell
B cell
Monocyte
NK cell
d
# of eGenes with sig. int. beta (q < 0.05)
B
CD4+ T
CD8+ T
Monocyte
NK
e
# of eGenes with sig. int. beta (q < 0.05)
PC1
PC2
PC3
PC4
PC5
PC6
f
PCs
77
292
78
Cell types
g
PC1
39
PC1 and monocyte-dependent
209
Monocyte
42
i
PC3
17
PC3 and B cell-dependent
44
B cell
43
h
Mono
other
EIF5A (log2 counts + 1)
T/T
T/C
C/C
rs1054378
PC1: Low Med High
j
B cell
other
SERPINB6 (log2 counts + 1)
C/C
C/T
T/T
rs62391542
PC3: Low Med High

Supplementary Figure 14: Single-cell eQTL analysis in mixed cell types. **a,** UMAP of unstimulated (mock-treated) PBMCs from Randolph, et al. Cells are colored by five major cell type annotations from the original study. **b**, UMAPs colored by expression of major lineage defining markers: *CD3D* for T cells, *CD8A* for CD8+ T cells, *MS4A1* for B cells, *CD14* for monocytes, and *FCGR3A* for some NK cells and monocytes. Cells are colored from low (blue) to high (yellow) expression. **c,** (left) Violin plots of cell types' distributions along batch-corrected PC to which they are strongly associated, as shown in the heatmap (right). The heatmap is colored by betas from logistic regression models using the six PCs to predict cells' membership in each cell type. Betas are scaled within each cell type. **d**, Bar plot of the number of eGenes with significant interactions with each discrete cell type in univariate PME models or **e**, with each PC in a multivariate PME model ($q < 0.05$). **f**, Venn diagram of overlapping and distinct eQTLs between the 6-PC and five individual cell type analyses. **g**, Venn diagram comparing PC1 and monocyte-dependent eQTLs. **h,** eQTL for *EIF5A* plotted for monocytes vs. other cells on the left, or by tertiles of PC1 on the right. **i**, Venn diagram comparing PC3 and B cell-dependent eQTLs. **j**, eQTL for *SERPINB6* plotted for B cells vs. other cells on the left, or by tertiles of PC3 on the right. For all box plots, each point represents the average log2(UMI counts + 1) across all cells in the indicated subset of cells in a donor (n = 89), grouped by genotype. Box plots show median (horizontal bar), 25th and 75th percentiles (lower and upper bounds of the box, respectively) and 1.5 times the IQR (or minimum/maximum values if they fall within that range; end of whiskers).

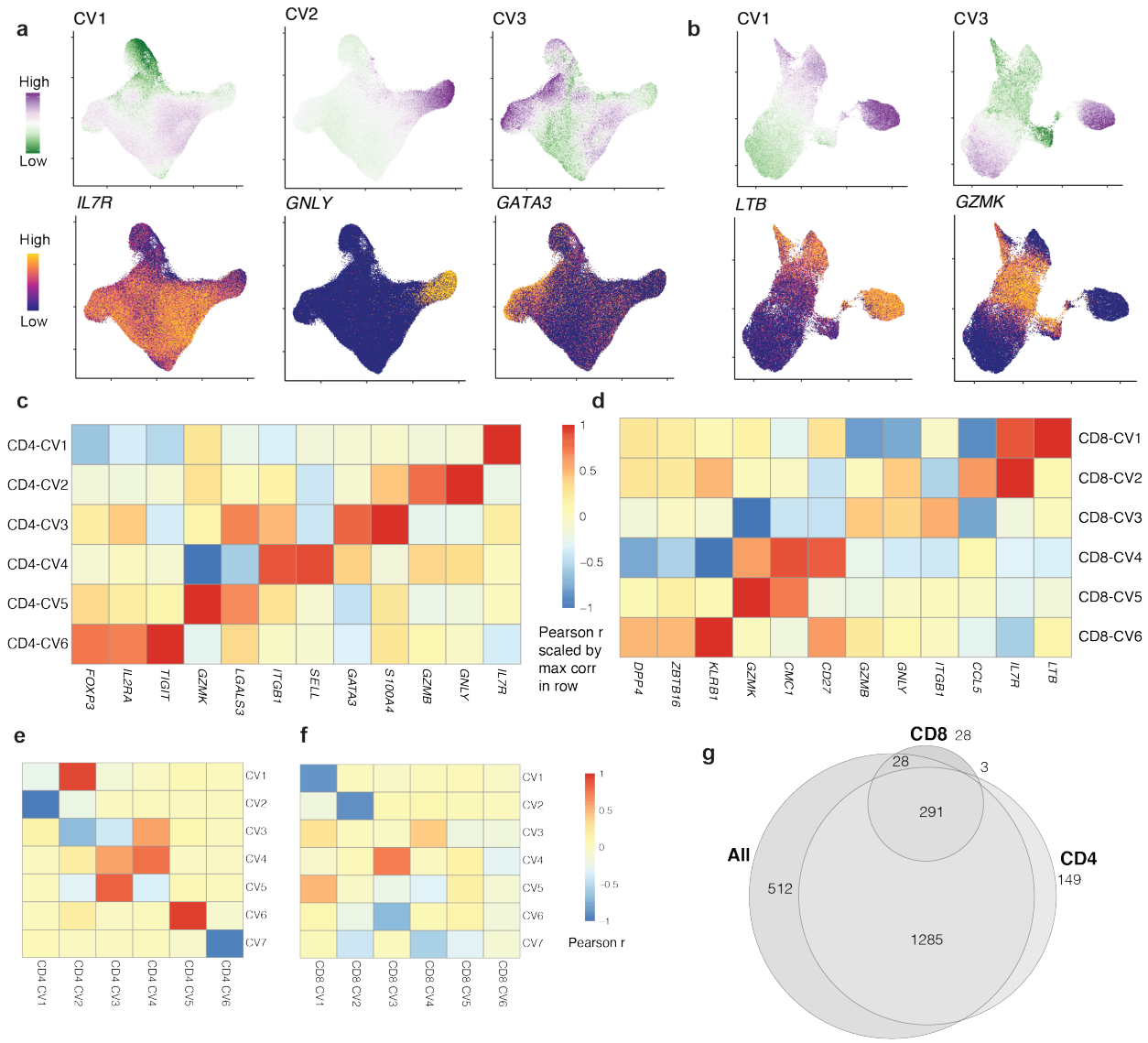

Supplementary Figure 15: State-dependent eQTL analysis within lineages. **a**, UMAP of CD4+ memory T cells colored by CD4-CVs 1-3 (top) or by the expression of CV-correlated marker genes (bottom). **b,** UMAP of CD8+ memory T cells colored by CD8-CVs 1 and 3 (top) and marker genes (bottom). CV UMAPs are colored from low (green) to high (purple) CV score. Marker gene UMAPs are colored from low (blue) to high (yellow) gene expression. **c,** Heatmap of correlations between CD4-CVs or **d,** CD8-CVs and marker genes. Heatmap is colored based on Pearson r scaled within each CV relative to the maximum value and centered at 0. **e,** Heatmap of correlations between CD4-CVs or **f**, CD8-CVs and all-memory-T-cell CVs. Heatmap is colored based on Pearson r. **g**, Venn diagram of significant state-dependent eGenes ($q < 0.05$) overlapping between the 7-memory-CV, 7-CD4-CV, and 7-CD8-CV multivariate PME interaction models.

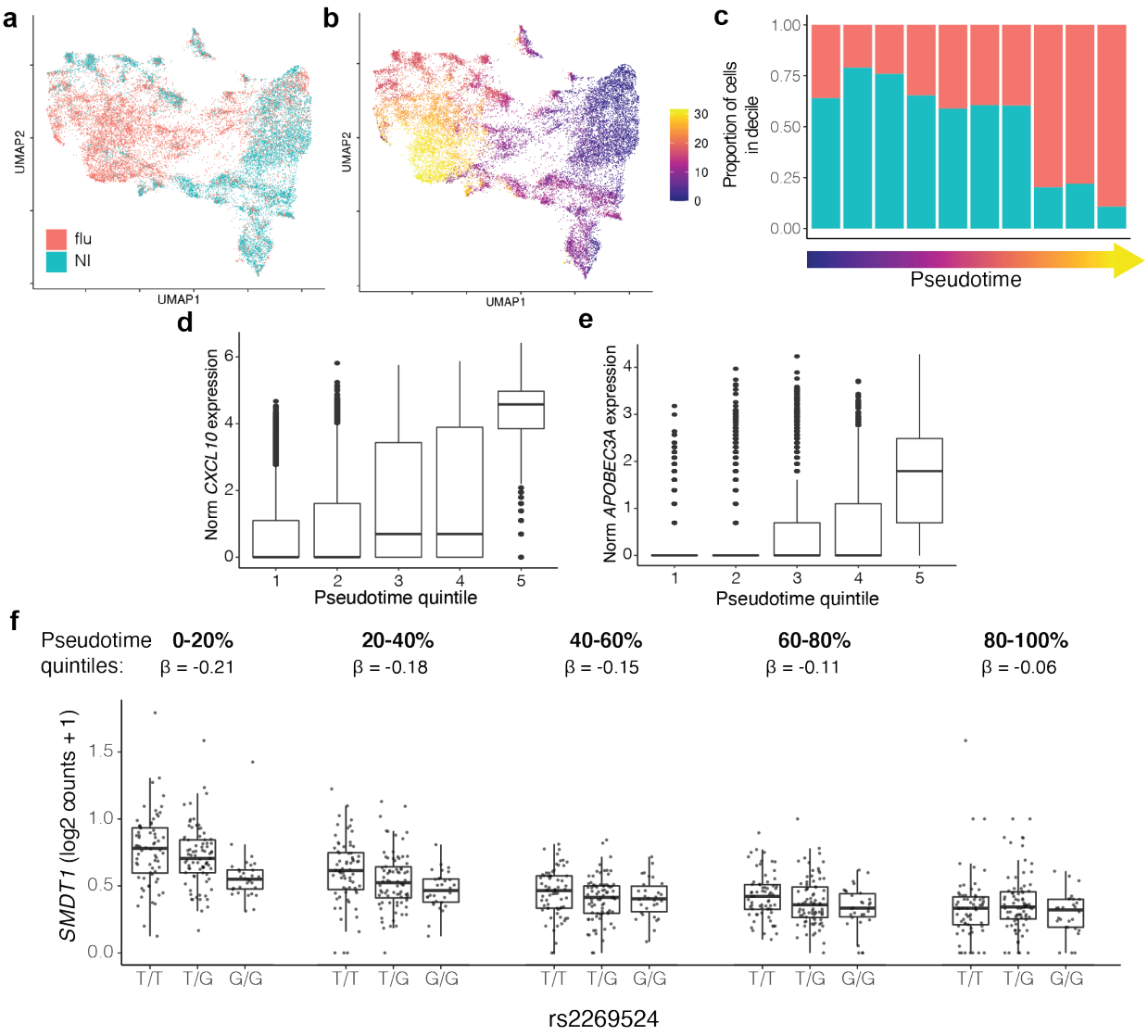

Supplementary Figure 16: eQTL interactions with an interferon-response trajectory in monocytes. a, UMAP of monocytes from Randolph, et al. colored by condition. NI = mock-treated, flu = exposed to influenza A virus. **b,** UMAP of monocytes from Randolph, et al. colored by trajectory pseudotime. This pseudotime was defined as a principal curve along a DDRTree trajectory **c**, Proportion of cells from flu and NI conditions along the trajectory. Each bar represents one decile of pseudotime, and the colors correspond to the proportion of cells in that decile from flu (orange) or mock-treated (turquoise) samples. **d,** Boxplots of normalized *CXCL10* and **e,** *APOBEC3A* expression in each quintile along the trajectory. Boxplots in d-f show median (horizontal bar), 25th and 75th percentiles (lower and upper bounds of the box, respectively) and 1.5 times the IQR (or minimum/maximum values if they fall within that range; end of whiskers) n = 24,783 for all box plots. **f**, rs2269524 eQTL for *SMDT1* in each quintile along the trajectory. Betas are the average single-cell beta across cells in the quintile.

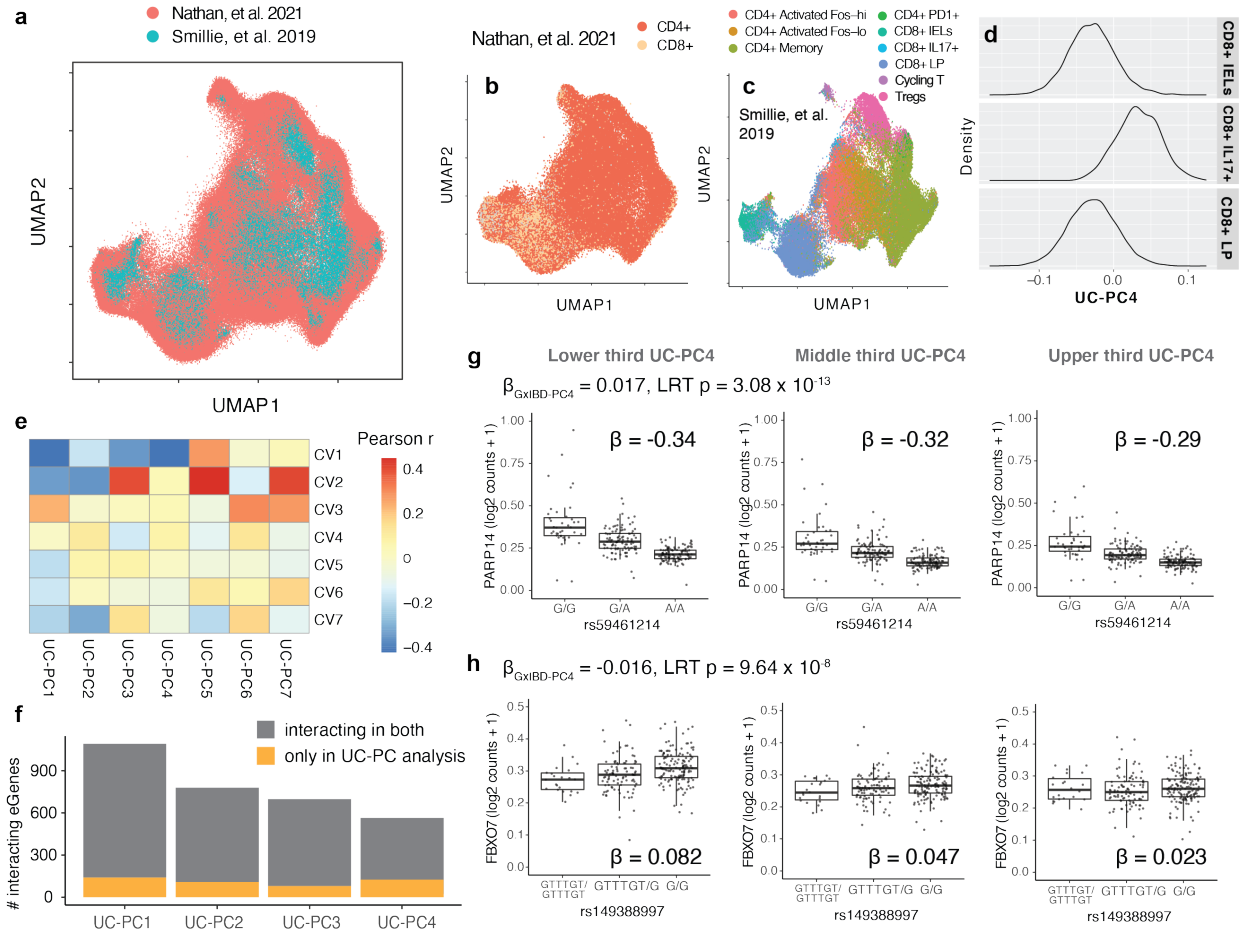

Supplementary Figure 17: eQTL interactions through projections onto colon T cell states in ulcerative colitis. a, UMAP of cells from the healthy blood memory T cell dataset (Nathan et al. 2021, orange) projected onto a reference of ulcerative colitis (UC) colon T cells (Smillie, et al. 2019, turquoise). **b,** UMAP of cells from Nathan, et al. colored by major lineage. **c,** UMAP of T cells from Smillie, et al. colored by clusters. **d,** Distribution of colon T cells' scores along PC4 from Smillie, et al. Each graph depicts the distribution of UC-PC4 scores for cells from each of the CD8+ clusters. **e,** Heatmap of Pearson correlations between CVs from blood memory T cells and UC-PCs. **f,** Bar plot of state-dependent eQTLs for each UC-PC, estimated by modeling eQTLs in memory T cells from Nathan et al. projected onto each PC in separate univariate PME interaction models. The yellow portion of each bar represents the interacting eGenes that were only found to be state-dependent in the UC-PC analyses. **g,** Examples of eQTLs for *PARP14* and **h,** *FBXO7*. Box plots show eQTL effect for cells in the bottom (left), middle (center), and top (right) thirds of CV1 scores. Each point in a box plot represents the average log2(UMI counts + 1) across all cells in the indicated subset of cells in a donor (n = 259), grouped by genotype. Box plots show median (horizontal bar), 25th and 75th percentiles (lower and upper bounds of the box, respectively) and 1.5 times the IQR (or minimum/maximum values if they fall within that range; end of whiskers). Beta is calculated through a PME model run on only cells in that tertile. P

value is calculated from a likelihood ratio test comparing models with and without GxCV1 interactions.

Legends for Supplementary Tables 1-48

Supplementary Table 1. Pseudobulk memory T cell eQTLs in a Peruvian cohort. (See Nathan_etal_SuppTables.xlsx, tab 1)

Lead eQTL variant for each eGene tested in a linear model of pseudobulk gene expression assayed in memory T cells from a Peruvian cohort. All SNP coordinates are from GRCh38. The model adjusts for donor's age and sex, 5 genotype PCs, and 45 PEER factors. P values are from FastQTL beta approximation-based permutation.

Supplementary Table 2. Ancestry-specific eQTL variants. (See Nathan_etal_SuppTables.xlsx, tab 2)

eQTL variants in the Peruvian dataset driven by variants that are rare (MAF < 0.05) in 1KG EUR population.

Supplementary Table 3. Conditional pseudobulk memory T cell eQTLs. (See Nathan_etal_SuppTables.xlsx, tab 3)

Secondary eQTL variant for each eGene tested in a linear model of pseudobulk gene expression assayed in memory T cells from a Peruvian cohort, after regressing out the lead effect. The model adjusts for donor's age and sex, 5 genotype PCs, and 45 PEER factors. P values are from FastQTL beta approximation-based permutation.

Supplementary Table 4. Blueprint cell-type-specific concordance of pseudobulk eQTLs (See Nathan_etal_SuppTables.xlsx, tab 4)

Comparison of eQTL effects between pseudobulk memory T cells and Blueprint naïve T cells, monocytes, and neutrophils. Effects are marked as either significant in both studies in the same direction (green) or opposite direction (red), not significant in the Blueprint study (yellow), or not measured in the Blueprint study (white).

Supplementary Table 5. CV markers and Gene set enrichment (See Nathan_etal_SuppTables.xlsx, tab 5)

a, Top 5 marker genes and proteins for each of the top 7 CVs, based on Pearson correlation with each batch-corrected CV. b, Top 10 gene sets enriched for each CV based on genes' loadings. P values and enrichment statistics are from the fgsea R package.

Supplementary Table 6. Average CV scores by memory T cell cluster (See Nathan_etal_SuppTables.xlsx, tab 6)

Average score along each CV for cells in each cluster. Clusters were defined in Nathan, et al. by projecting cells into a low-dimensional embedding based on CCA of paired mRNA and surface protein, constructing a shared nearest neighbor graph, and conducting Louvain clustering at resolution = 2. Clusters were annotated based on differentially expressed genes and proteins.

Supplementary Table 7. Single-cell Poisson model of memory T cell eQTLs. (See Nathan_etal_SuppTables.xlsx, tab 7)

eQTL effects calculated with the PME model (without cell state interactions) for significant eGenes and lead variants identified in the pseudobulk analysis. The model adjusts for donor's age and sex, percent MT UMIs and number of UMIs per cell, 5 genotype PCs, 5 expression PCs, and has random effects for donor and library preparation pool. P values are from an LRT comparing the model with and without the genotype term.

Supplementary Table 8. Single-cell Poisson model of memory T cell eQTLs' interaction with prior TB status. (See Nathan_etal_SuppTables.xlsx, tab 8)

eQTL interactions with donors' prior TB progression status calculated with the PME model for significant eGenes and lead variants identified in the pseudobulk analysis. The model adjusts for donor's age and sex, percent MT UMIs and number of UMIs per cell, 5 genotype PCs, 5 expression PCs, and has random effects for donor and library preparation pool. P values are from an LRT comparing the model with and without the TB status term.

Supplementary Table 9. Single-cell Poisson model of memory T cell eQTLs' dependence on CD4+ state. (See Nathan_etal_SuppTables.xlsx, tab 9)

eQTL interactions with cells' CD4+ state calculated with the PME model for significant eGenes and lead variants identified in the pseudobulk analysis. CD4+ cells were defined based on normalized surface protein expression measured in CITE-seq (CD4+CD8-). The model adjusts for donor's age and sex, percent MT UMIs and number of UMIs per cell, 5 genotype PCs, 5 expression PCs, and has random effects for donor and library preparation pool. Model p values are from an LRT comparing the model with and without the CD4+ state interaction term. Interaction-term p values are from Wald z scores of the betas.

Supplementary Table 10. Pseudobulk memory T cell eQTLs in CD4+ cells only. (See Nathan_etal_SuppTables.xlsx, tab 10)

eQTLs in CD4+ memory T cells calculated with a pseudobulk linear model in FastQTL for significant eGenes and lead variants identified in the pseudobulk analysis. CD4+ cells were defined based on normalized surface protein expression measured in CITE-seq (CD4+CD8-). The model adjusts for donor's age and sex, 5 genotype PCs, and 45 PEER factors and we calculated a nominal P value for the genotype effect.

Supplementary Table 11. Single-cell Poisson model of memory T cell eQTLs in CD4+ cells only. (See Nathan_etal_SuppTables.xlsx, tab 11)

eQTL in CD4+ memory T cells calculated with the PME model for significant eGenes and lead variants identified in the pseudobulk analysis. CD4+ cells were defined based on normalized surface protein expression measured in CITE-seq (CD4+CD8-). The model adjusts for donor's age and sex, percent MT UMIs and number of UMIs per cell, 5 genotype PCs, 5 expression PCs, and has random effects for donor and library preparation pool. Model p values are from an LRT comparing the model with and without genotype term. Interaction-term p values are from Wald z scores of the betas.

Supplementary Table 12. Single-cell Poisson model of memory T cell eQTLs' dependence on CD8+ state. (See Nathan_etal_SuppTables.xlsx, tab 12)

eQTL interactions with cells' CD8+ state calculated with the PME model for significant eGenes and lead variants identified in the pseudobulk analysis. CD8+ cells were defined based on normalized surface protein expression measured in CITE-seq (CD4-CD8+). The model adjusts for donor's age and sex, percent MT UMIs and number of UMIs per cell, 5 genotype PCs, 5 expression PCs, and has random effects for donor and library preparation pool. Model p values are from an LRT comparing the model with and without the CD8+ state interaction term. Interaction-term p values are from Wald z scores of the betas.

Supplementary Table 13. Single-cell Poisson model of memory T cell eQTLs in CD8+ cells only. (See Nathan_etal_SuppTables.xlsx, tab 13)

eQTL in CD8+ memory T cells calculated with the PME model for significant eGenes and lead variants identified in the pseudobulk analysis. CD8+ cells were defined based on normalized surface protein expression measured in CITE-seq (CD4-CD8+). The model adjusts for donor's age and sex, percent MT UMIs and number of UMIs per cell, 5 genotype PCs, 5 expression PCs, and has random effects for donor and library preparation pool. Model p values are from an LRT comparing the model with and without genotype term. Interaction-term p values are from Wald z scores of the betas.

Supplementary Table 14. Single-cell linear model of memory T cell eQTLs. (See Nathan_etal_SuppTables.xlsx, tab 14)

eQTL effects calculated with the LME model (without cell state interactions) for significant eGenes and lead variants identified in the pseudobulk analysis. The model adjusts for donor's age and sex, percent MT UMIs and number of UMIs per cell, 5 genotype PCs, 5 expression PCs, and has random effects for donor and library preparation pool. Model p values are from an LRT comparing the model with and without the genotype term. Interaction-term p values are from Wald z scores of the betas.

Supplementary Table 15. Single-cell linear model of memory T cell eQTLs' dependence on CD4+ state. (See Nathan_etal_SuppTables.xlsx, tab 15)

eQTL interactions with cells' CD4+ state calculated with the LME model for significant eGenes and lead variants identified in the pseudobulk analysis. CD4+ cells were defined based on normalized surface protein expression measured in CITE-seq (CD4+CD8-). The model adjusts for donor's age and sex, percent MT UMIs and number of UMIs per cell, 5 genotype PCs, 5 expression PCs, and has random effects for donor and library preparation pool. Model p values are from an LRT comparing the model with and without the CD4+ state interaction term. Interaction-term p values are from Wald z scores of the betas.

Supplementary Table 16. Single-cell Poisson model of memory T cell eQTLs' dependence on CV1. (See Nathan_etal_SuppTables.xlsx, tab 16)

eQTL interactions with cells' CV1 calculated with the PME model for significant eGenes and lead variants identified in the pseudobulk analysis. The model adjusts for donor's age and sex, percent MT UMIs and number of UMIs per cell, 5 genotype PCs, 5 expression PCs, and has random effects for donor and library preparation pool. Model p values are from an LRT comparing the model with and without the CV1 interaction term. Interaction-term p values are from Wald z scores of the betas.

Supplementary Table 17. Single-cell negative binomial model of memory T cell eQTLs' dependence on CV1. (See Nathan_etal_SuppTables.xlsx, tab 17)

eQTL interactions with cells' CV1 calculated with the negative binomial mixed model for significant eGenes and lead variants identified in the pseudobulk analysis. The model adjusts for donor's age and sex, percent MT UMIs and number of UMIs per cell, 5 genotype PCs, 5 expression PCs, and has random effects for donor and library preparation pool. Model p values are from an LRT comparing the model with and without the CV1 interaction term. Interaction-term p values are from Wald z scores of the betas.

Supplementary Table 18. Single-cell Poisson model of memory T cell eQTLs' dependence on CV2. (See Nathan_etal_SuppTables.xlsx, tab 18)

eQTL interactions with cells' CV2 calculated with the PME model for significant eGenes and lead variants identified in the pseudobulk analysis. The model adjusts for donor's age and sex, percent MT UMIs and number of UMIs per cell, 5 genotype PCs, 5 expression PCs, and has random effects for donor and library preparation pool. Model p values are from an LRT comparing the model with and without the CV2 interaction term. Interaction-term p values are from Wald z scores of the betas.

Supplementary Table 19. Single-cell Poisson model of memory T cell eQTLs' dependence on Treg state. (See Nathan_etal_SuppTables.xlsx, tab 19)

eQTL interactions with Tregs calculated with the PME model for significant eGenes and lead variants identified in the pseudobulk analysis. The Tregs were identified through clustering in Nathan, et al. The model adjusts for donor's age and sex, percent MT UMIs and number of UMIs per cell, 5 genotype PCs, 5 expression PCs, and has random effects for donor and library preparation pool. Model p values are from an LRT comparing the model with and without the Treg interaction term. Interaction-term p values are from Wald z scores of the betas.

Supplementary Table 20. Single-cell Poisson model of memory T cell eQTLs' dependence on CVs 1-7. (See Nathan_etal_SuppTables.xlsx, tab 20)

eQTL interactions with CVs1-7 calculated with the PME model for significant eGenes and lead variants identified in the pseudobulk analysis. The model adjusts for donor's age and sex, percent MT UMIs and number of UMIs per cell, 5 genotype PCs, 5 expression PCs, and has random effects for donor and library preparation pool. Model p

values are from an LRT comparing the model with and without the CV1-7 interaction terms. Interaction-term p values are from Wald z scores of the betas.

Supplementary Table 21. Single-cell Poisson model of memory T cell eQTLs' dependence on CV3. (See Nathan_etal_SuppTables.xlsx, tab 21)
eQTL interactions with cells' CV3 calculated with the PME model for significant eGenes and lead variants identified in the pseudobulk analysis. The model adjusts for donor's age and sex, percent MT UMIs and number of UMIs per cell, 5 genotype PCs, 5 expression PCs, and has random effects for donor and library preparation pool. Model p values are from an LRT comparing the model with and without the CV3 interaction term. Interaction-term p values are from Wald z scores of the betas.

Supplementary Table 22. Single-cell Poisson model of memory T cell eQTLs' dependence on CV4. (See Nathan_etal_SuppTables.xlsx, tab 22)
eQTL interactions with cells' CV4 calculated with the PME model for significant eGenes and lead variants identified in the pseudobulk analysis. The model adjusts for donor's age and sex, percent MT UMIs and number of UMIs per cell, 5 genotype PCs, 5 expression PCs, and has random effects for donor and library preparation pool. Model p values are from an LRT comparing the model with and without the CV4 interaction term. Interaction-term p values are from Wald z scores of the betas.

Supplementary Table 23. Single-cell Poisson model of memory T cell eQTLs' dependence on CV5. (See Nathan_etal_SuppTables.xlsx, tab 23)
eQTL interactions with cells' CV5 calculated with the PME model for significant eGenes and lead variants identified in the pseudobulk analysis. The model adjusts for donor's age and sex, percent MT UMIs and number of UMIs per cell, 5 genotype PCs, 5 expression PCs, and has random effects for donor and library preparation pool. P values are from an LRT comparing the model with and without the CV5 interaction term.

Supplementary Table 24. Single-cell Poisson model of memory T cell eQTLs' dependence on CV6. (See Nathan_etal_SuppTables.xlsx, tab 24)
eQTL interactions with cells' CV6 calculated with the PME model for significant eGenes and lead variants identified in the pseudobulk analysis. The model adjusts for donor's age and sex, percent MT UMIs and number of UMIs per cell, 5 genotype PCs, 5 expression PCs, and has random effects for donor and library preparation pool. Model p values are from an LRT comparing the model with and without the CV6 interaction term. Interaction-term p values are from Wald z scores of the betas.

Supplementary Table 25. Single-cell Poisson model of memory T cell eQTLs' dependence on CV7. (See Nathan_etal_SuppTables.xlsx, tab 25)
eQTL interactions with cells' CV7 calculated with the PME model for significant eGenes and lead variants identified in the pseudobulk analysis. The model adjusts for donor's age and sex, percent MT UMIs and number of UMIs per cell, 5 genotype PCs, 5

expression PCs, and has random effects for donor and library preparation pool. Model p values are from an LRT comparing the model with and without the CV7 interaction term. Interaction-term p values are from Wald z scores of the betas.

Supplementary Table 26. Single-cell Poisson model of memory T cell eQTLs' dependence on CV8. (See Nathan_etal_SuppTables.xlsx, tab 26)

eQTL interactions with cells' CV8 calculated with the PME model for significant eGenes and lead variants identified in the pseudobulk analysis. The model adjusts for donor's age and sex, percent MT UMIs and number of UMIs per cell, 5 genotype PCs, 5 expression PCs, and has random effects for donor and library preparation pool. Model p values are from an LRT comparing the model with and without the CV8 interaction term. Interaction-term p values are from Wald z scores of the betas.

Supplementary Table 27. Single-cell Poisson model of memory T cell eQTLs' dependence on CV9. (See Nathan_etal_SuppTables.xlsx, tab 27)

eQTL interactions with cells' CV9 calculated with the PME model for significant eGenes and lead variants identified in the pseudobulk analysis. The model adjusts for donor's age and sex, percent MT UMIs and number of UMIs per cell, 5 genotype PCs, 5 expression PCs, and has random effects for donor and library preparation pool. Model p values are from an LRT comparing the model with and without the CV9 interaction term. Interaction-term p values are from Wald z scores of the betas.

Supplementary Table 28. Single-cell Poisson model of memory T cell eQTLs' dependence on CV10. (See Nathan_etal_SuppTables.xlsx, tab 28)

eQTL interactions with cells' CV10 calculated with the PME model for significant eGenes and lead variants identified in the pseudobulk analysis. The model adjusts for donor's age and sex, percent MT UMIs and number of UMIs per cell, 5 genotype PCs, 5 expression PCs, and has random effects for donor and library preparation pool. Model p values are from an LRT comparing the model with and without the CV10 interaction term. Interaction-term p values are from Wald z scores of the betas.

Supplementary Table 29. Single-cell Poisson model of memory T cell eQTLs' dependence on CV11. (See Nathan_etal_SuppTables.xlsx, tab 29)

eQTL interactions with cells' CV11 calculated with the PME model for significant eGenes and lead variants identified in the pseudobulk analysis. The model adjusts for donor's age and sex, percent MT UMIs and number of UMIs per cell, 5 genotype PCs, 5 expression PCs, and has random effects for donor and library preparation pool. Model p values are from an LRT comparing the model with and without the CV11 interaction term. Interaction-term p values are from Wald z scores of the betas.

Supplementary Table 30. Single-cell Poisson model of memory T cell eQTLs' dependence on CV12. (See Nathan_etal_SuppTables.xlsx, tab 30)

eQTL interactions with cells' CV12 calculated with the PME model for significant eGenes and lead variants identified in the pseudobulk analysis. The model adjusts for donor's age and sex, percent MT UMIs and number of UMIs per cell, 5 genotype PCs, 5 expression PCs, and has random effects for donor and library preparation pool. Model p

values are from an LRT comparing the model with and without the CV12 interaction term. Interaction-term p values are from Wald z scores of the betas.

Supplementary Table 31. Single-cell Poisson model of memory T cell eQTLs' dependence on CV13. (See Nathan_etal_SuppTables.xlsx, tab 31)

eQTL interactions with cells' CV13 calculated with the PME model for significant eGenes and lead variants identified in the pseudobulk analysis. The model adjusts for donor's age and sex, percent MT UMIs and number of UMIs per cell, 5 genotype PCs, 5 expression PCs, and has random effects for donor and library preparation pool. Model p values are from an LRT comparing the model with and without the CV13 interaction term. Interaction-term p values are from Wald z scores of the betas.

Supplementary Table 32. Single-cell Poisson model of memory T cell eQTLs' dependence on CV14. (See Nathan_etal_SuppTables.xlsx, tab 32)

eQTL interactions with cells' CV14 calculated with the PME model for significant eGenes and lead variants identified in the pseudobulk analysis. The model adjusts for donor's age and sex, percent MT UMIs and number of UMIs per cell, 5 genotype PCs, 5 expression PCs, and has random effects for donor and library preparation pool. Model p values are from an LRT comparing the model with and without the CV14 interaction term. Interaction-term p values are from Wald z scores of the betas.

Supplementary Table 33. Single-cell Poisson model of memory T cell eQTLs' dependence on CV15. (See Nathan_etal_SuppTables.xlsx, tab 33)

eQTL interactions with cells' CV15 calculated with the PME model for significant eGenes and lead variants identified in the pseudobulk analysis. The model adjusts for donor's age and sex, percent MT UMIs and number of UMIs per cell, 5 genotype PCs, 5 expression PCs, and has random effects for donor and library preparation pool. Model p values are from an LRT comparing the model with and without the CV15 interaction term. Interaction-term p values are from Wald z scores of the betas.

Supplementary Table 34. Single-cell Poisson model of non-pseudobulk-significant memory T cell eQTLs' dependence on CVs 1-7. (See Nathan_etal_SuppTables.xlsx, tab 34)

eQTL interactions with CVs1-7 calculated with the PME model for non-significant eGenes and lead variants identified in the pseudobulk analysis. The model adjusts for donor's age and sex, percent MT UMIs and number of UMIs per cell, 5 genotype PCs, 5 expression PCs, and has random effects for donor and library preparation pool. Model p values are from an LRT comparing the model with and without the CV1-7 interaction terms. Interaction-term p values are from Wald z scores of the betas.

Supplementary Table 35. GO Term enrichment in eGene clusters. (See Nathan_etal_SuppTables.xlsx, tab 35)

Top 5 Gene Ontology gene sets enriched for overlap with eGenes in each of the ten eGene clusters. These clusters were defined through Louvain clustering on the betas for each eGene's interactions with each of the 7 CVs, scaled relative to the largest-

magnitude value and with signs corrected to be relative to the main genotype effect for that eGene. P values are from a one-sided Fisher test.

Supplementary Table 36. HOMER analysis of CV-interacting eGenes. (See Nathan_etal_SuppTables.xlsx, tab 36)

a, Top 5 transcription factor binding motifs enriched in the promoters of eGenes interacting with each CV in the multivariate 7-CV model. in variants associated with traits in the GWAS Catalog. b, Top 5 transcription factor binding motifs enriched in the +/- 20bp window around the lead SNP for eGenes interacting with each CV in the multivariate 7-CV model.

Supplementary Table 37. Single-cell Poisson model of memory T cell eQTLs' dependence on mRNA PCs 1-7. (See Nathan_etal_SuppTables.xlsx, tab 37)

eQTL interactions with mRNA PCs 1-7 calculated with the PME model for significant eGenes and lead variants identified in the pseudobulk analysis. The model adjusts for donor's age and sex, percent MT UMIs and number of UMIs per cell, 5 genotype PCs, 5 expression PCs, and has random effects for donor and library preparation pool. Model p values are from an LRT comparing the model with and without the mRNA PC1-7 interaction terms. Interaction-term p values are from Wald z scores of the betas.

Supplementary Table 38. Single-cell Poisson model of memory T cell eQTLs' dependence on protein PCs 1-7. (See Nathan_etal_SuppTables.xlsx, tab 38)

eQTL interactions with protein PCs 1-7 calculated with the PME model for significant eGenes and lead variants identified in the pseudobulk analysis. The model adjusts for donor's age and sex, percent MT UMIs and number of UMIs per cell, 5 genotype PCs, 5 expression PCs, and has random effects for donor and library preparation pool. Model p values are from an LRT comparing the model with and without the protein PC1-7 interaction terms. Interaction-term p values are from Wald z scores of the betas.

Supplementary Table 39. Single-cell Poisson model of conditional/secondary memory T cell eQTLs' dependence on CVs 1-7. (See Nathan_etal_SuppTables.xlsx, tab 39)

eQTL interactions with CVs 1-7 calculated with the PME model for significant eGenes and conditional/secondary variants identified in the pseudobulk analysis. The model adjusts for donor's age and sex, percent MT UMIs and number of UMIs per cell, 5 genotype PCs, 5 expression PCs, and has random effects for donor and library preparation pool. Model p values are from an LRT comparing the model with and without the CV1-7 interaction terms. Interaction-term p values are from Wald z scores of the betas.

Supplementary Table 40. GO Term enrichment in state-dependent eGenes. (See Nathan_etal_SuppTables.xlsx, tab 40)

Top 10 Gene Ontology gene sets enriched for overlap with eGenes interacting with each of the seven CVs in the multivariate model. P values are from a one-sided Fisher test.

Supplementary Table 41. eQTL enrichment among GWAS variants by trait. (See Nathan_etal_SuppTables.xlsx, tab 41)

Enrichments of memory T cell eQTLs in variants associated with traits in the GWAS Catalog. Variants were considered to be overlapping if they had $r^2 > .5$ in both 1KG EUR and PEL populations. P values are from a Fisher test comparing the proportion of eQTLs in a trait's GWAS variants to the proportion of eQTLs in GWAS variants for all other GWAS Catalog traits.

Supplementary Table 42. State-dependent eQTL enrichment among GWAS variants by trait. (See Nathan_etal_SuppTables.xlsx, tab 42)

Enrichments of state-dependent memory T cell eQTLs in variants associated with traits in the GWAS Catalog. Variants were considered to be overlapping if they had $r^2 > .5$ in both 1KG EUR and PEL populations. P values are from a Fisher test comparing the proportion of state-dependent eQTLs in a trait's GWAS variants to the proportion of non-state-dependent eQTLs in GWAS variants for that trait.

Supplementary Table 43. Single-cell Poisson model of PBMC eQTLs' dependence on mRNA PCs 1-6. (See Nathan_etal_SuppTables.xlsx, tab 43)

eQTL interactions with mRNA PCs 1-6 calculated with the PME model for significant eGenes and lead variants identified in the PBMC pseudobulk analysis. The model adjusts for donor's age, percent MT UMIs and number of UMIs per cell, 5 genotype PCs, 5 expression PCs, and has random effects for donor and batch. Model p values are from an LRT comparing the model with and without the mRNA PC1-6 interaction terms. Interaction-term p values are from Wald z scores of the betas.

Supplementary Table 44. Single-cell Poisson model of PBMC eQTLs' dependence on major cell types. (See Nathan_etal_SuppTables.xlsx, tab 44)

eQTL interactions with major cell types (CD4+ T, CD8+ T, B, NK, monocytes) calculated with separate univariate PME models for significant eGenes and lead variants identified in the PBMC pseudobulk analysis. The models adjust for donor's age, percent MT UMIs and number of UMIs per cell, 5 genotype PCs, 5 expression PCs, and has random effects for donor and batch. Model p values are from an LRT comparing the model with and without the respective cell type interaction term. Interaction-term p values are from Wald z scores of the betas.

Supplementary Table 45. Single-cell Poisson model of memory T cell eQTLs' dependence on CD4 CVs 1-6. (See Nathan_etal_SuppTables.xlsx, tab 45)

eQTL interactions with CD4 CVs 1-6 calculated with the PME model for significant eGenes and lead variants identified in the pseudobulk analysis. The model adjusts for donor's age and sex, percent MT UMIs and number of UMIs per cell, 5 genotype PCs, 5 expression PCs, and has random effects for donor and library preparation pool. Model p values are from an LRT comparing the model with and without the CD4 CVs 1-6 interaction terms. Interaction-term p values are from Wald z scores of the betas.

Supplementary Table 46. Single-cell Poisson model of memory T cell eQTLs' dependence on CD8 CVs 1-6. (See Nathan_etal_SuppTables.xlsx, tab 46)

eQTL interactions with CD8 CVs 1-6 calculated with the PME model for significant eGenes and lead variants identified in the pseudobulk analysis. The model adjusts for donor's age and sex, percent MT UMIs and number of UMIs per cell, 5 genotype PCs, 5 expression PCs, and has random effects for donor and library preparation pool. Model p values are from an LRT comparing the model with and without the CD8 CVs 1-6 interaction terms. Interaction-term p values are from Wald z scores of the betas.

Supplementary Table 47. Single-cell Poisson model of monocyte eQTLs' dependence on an interferon response trajectory. (See Nathan_etal_SuppTables.xlsx, tab 47)

eQTL interactions with an interferon trajectory calculated with the PME model for significant eGenes and lead variants identified in the monocyte or PBMC pseudobulk analysis. The model adjusts for donor's age, percent MT UMIs and number of UMIs per cell, 5 genotype PCs, 5 expression PCs, and has random effects for donor and batch. Model p values are from an LRT comparing the model with and without the trajectory interaction term. Interaction-term p values are from Wald z scores of the betas.

Supplementary Table 48. Single-cell Poisson model of memory T cell eQTLs' dependence on UC colon T cell PCs 1-4. (See Nathan_etal_SuppTables.xlsx, tab 48)

eQTL interactions with UC-PCs 1-4 (Smillie, et al.) calculated with separate univariate PME models for significant eGenes and lead variants identified in the pseudobulk analysis. The model adjusts for donor's age and sex, percent MT UMIs and number of UMIs per cell, 5 genotype PCs, 5 expression PCs, and has random effects for donor and library preparation pool. Model p values are from an LRT comparing the model with and without the respective UC-PC. Interaction-term p values are from Wald z scores of the betas.